Satellite-derived changes in floodplain productivity and freshwater habitats in northern Australia (1991–2019)

Author

Ndehedehe, CE, Burford, MA, Stewart-Koster, B, Bunn, SE

Published

Journal Title

Version

Submitted Manuscript (SM)

DOI

Rights statement

Downloaded from

Griffith Research Online

Satellite-derived changes in floodplain productivity and freshwater habitats in northern Australia (1991-2019)

Christopher E. Ndehedehe[a], Michele. A. Burford[a], Ben Stewart-Koster[a], Stuart E. Bunn[a]

[a]*Australian Rivers Institute and Griffith School of Environment & Science, Griffith University, Nathan, Queensland 4111, Australia.*

Abstract

The ecological communities supported by freshwater habitats and wetlands that persist from floodplain inundation generate numerous cultural, recreational and economic values via commercial fisheries and other human uses of these habitats. However, the alteration of flow connectivity, degradation, and disruption of physical processes that sustain different levels of organisms (e.g., primary producers) are threats that affect aquatic biodiversity and the productivity of these habitats. Therefore, the large scale assessment of freshwater habits for proactive water resources planning and the development of climate change mitigation and resource management strategies is essential. However, such monitoring and assessment is complicated by the inaccessibility of many large wetland systems during times of inundation, making in-situ sampling impossible at a time when high levels of aquatic primary production are generating food and energy sources for higher order consumers. To understand the physical dynamics of aquatic primary producers and freshwater habitats ($1991 - 2019$) during such times in a large floodplain river in northern Australia (Gilbert catchment), this study integrated Landsat-derived modified normalised difference water index and normalised difference vegetation index in a classification tree model. Thereafter, key hydrological drivers (rainfall and river discharge) of floodplain productivity and connectivity were assessed using a range of multivariate techniques. Results show that the floodplain had a high aquatic plant biomass during the summer wet season based on the correlation between aquatic biomass accumulation (hot spots) and inundation ($r = 0.83$ @ phase lag < 1 month) during such period. River discharge ($r = 0.68$ @ lag=1 month) at downstream Gilbert catchment appear to be a relatively stronger indicator of hot spots of floodplain biomass accumulation as opposed to local rainfall ($r = 0.57$ @ lag=3 months). While the downstream discharge explains a significant proportion of variability in the leading orthogonal mode of rainfall ($r = 0.83$), statistical relationships developed between discharge/rainfall and the distribution of aquatic primary producers confirm

that both rivers (flow) and local rainfall are key optimal predictors of inundation and sites of primary producers with river flows being a better indicator of the latter. It is therefore argued that hydro-meteorological fluctuations will be key constraints on freshwater habitats and the growth of primary producers, albeit, human disturbance of flow can impact on floodplain productivity. As illustrated in this study, such constraints are reflected in the spatial patterns and changing characteristics (connectivity and spatial heterogeneity) of hot spots of primary producers and freshwater habitats (Palustrine, Lacustrine, and riverine ecosystems).

1. Introduction

Freshwater habitats such as rivers, lakes, streams, floodplain ecosystems, and vegetated wetlands are critical environmental resources that provide several ecosystem functions (e.g., Keddy et al., 2009). These freshwater systems and wetlands are highly valued because of their prominent roles in water quality improvement, provision of shelter for fish and native wildlife, flood water storage, drought relief for wildlife, recreation and tourism, and support for a range of terrestrial and aquatic biodiversity (e.g., Ward et al., 2014; Chen et al., 2014b; Tockner et al., 2010; Gidley, 2009; Bunn et al., 2006; Ozesmi and Bauer, 2002). In addition to this, they most often function as hot spots of biodiversity because of the wide spectrum of complexity in the heterogeneity and variations of habitats in space and time (e.g., Ward et al., 2016; Bunn et al., 2015; Karim et al., 2012; Tockner et al., 2010; Bunn et al., 2003). Consequently, because of these ecological, cultural and economic values and services, wetlands have been globally recognised as high prorities for conservation and management (e.g., Midwood and Chow-Fraser, 2010). Large-scale assessment of the productivity of these systems is therefore crucial to understanding (i) their response to multiple stressors and impacts on ecosystem processes and biodiversity (e.g., Davranche et al., 2010; Tockner et al., 2010) and (ii) important biogeochemical processes on floodplains, e.g., the interactions of green house gas with the atmosphere (e.g., Ward et al., 2014).

The abundance of higher order organisms (e.g., fish, invertebrates, and waterfowl) and aquatic plants (e.g., macrophytes, algae) in these freshwater systems during extreme wet periods (characterised by above-normal precipitation) and high flows result in the formation of a food web and highly productive habitats (e.g., Kingsford et al., 2014; Gidley, 2009; Bal-

combe and Arthington, 2009). However, extreme hydro-climatic (e.g., droughts), human (e.g., construction of dams and development of water infrastructure), and environmental (e.g., pollution) factors threaten freshwater habitats and affect aquatic biodiversity in streams and riverine systems (e.g., Kingsford et al., 2014; Bunn and Arthington, 2002). These existential threats are evidence by the global trend of degradation and destruction of floodplain wetland ecosystems, alteration of flow connectivity, and disruption of integrated physical processes that sustain different levels of organisms (e.g., primary and quaternary producers) who depend on these freshwater habitats (e.g., Ward et al., 2013; Davranche et al., 2010; Bunn et al., 2006; Bunn and Arthington, 2002).

The monitoring of floodplain productivity and dynamics in freshwater habitats, be it, riverine (e.g., rivers streams), lacustrine (large water holes in low elevation areas) or palustrine (swamps, intermittent floodplain water channels) systems (see, e.g., Ward et al., 2013) is therefore required to predict the impacts of hydro-meteorological fluctuations and the consequences of changes in flow dynamics on floodplain wetland ecosystems. This is essential among other things, for proactive water resources planning and the development of climate change mitigation and resource management strategies. Such monitoring and assessment is complicated by the inaccessibility of many large wetland systems during times of inundation, particularly in remote parts of the world. This can make in-situ sampling impossible at a time when high levels of aquatic primary production are generating food and energy sources for higher order consumers.

Several studies have highlighted and showcased the merits of optical and multi-mission satellite remote sensing techniques as the only viable alternative in large-scale environmental monitoring and assessment of natural systems, including floodplain wetlands. These optical systems, in addition to satellite gravity methods (e.g., Tapley et al., 2004) have been employed in multidisciplinary aspects of remote sensing hydrology and include, inventorying of wetlands and mapping of aquatic plants (e.g., Ward et al., 2016; Tockner et al., 2010; Midwood and Chow-Fraser, 2010; Ozesmi and Bauer, 2002), assessment of floodplain inundation and connectivity (e.g., Karim et al., 2018; Ward et al., 2013, 2014; Syvitski et al., 2012; Sakamoto et al., 2007), quantifying land-water storage (e.g., Ndehedehe, 2019; Kim et al., 2017; Lee et al., 2014; Frappart et al., 2012), monitoring and extraction of surface water in extensive floodplains (see, e.g., Tulbure and Broich, 2019; Normandin et al., 2018; Khandelwal et al., 2017; Feyisa et al., 2014; Xu, 2006), hydrological controls on surface vegetation (e.g., Ndehedehe et al., 2019b; Chen et al., 2014a), and analyses of extreme events (e.g., Ferreira et al.,

2018; Agutu et al., 2017), amongst others. As the threats to water resources are widening owing to a broad range of climate and environmental stressors such as land use change and agricultural expansion (Tulbure and Broich, 2019), the use of such methods to quantify the extent of aquatic primary producers during times of inundation is key to understanding the large-scale synergistic impacts of these stressors on floodplains.

Furthermore, methodological developments in the classification of water bodies from optical imageries, e.g., two-band thresholding and multiple-band index, and advances in satellite sensors have resulted in (i) an improved flood inundation mapping capability (see, e.g., Feyisa et al., 2014; Xu, 2006) and (ii) in the tracking of flood hydrographs and pathways, in addition to sedimentation patterns on a different time scales (Syvitski et al., 2012). However, there is limited large-scale remote sensing of primary producers centres in freshwater habitats, i.e., riverine, lacustrine, and palustrine systems with high biomass of aquatic plants (e.g., phytoplankton and macrophytes). While medium resolution images (e.g., Landsat) have not been fully explored to simultaneously quantify the spatio-temporal dynamics of these primary production centres (hot spots) and floodplain productivity on a large catchment-scale, the lack of standard field-based protocols and technological limitations in the mapping of aquatic vegetation have been identified (e.g., Zhao et al., 2013). Moreover, other past studies (see, e.g., Chen et al., 2018; Davranche et al., 2010; Cho et al., 2008) have argued that the overlapping spectral profiles of aquatic plants (emergent and floating macrophyte beds) at peak biomass and the limitations of the near-infrared wavelength in aquatic vegetation studies are key issues, warranting further research.

The aim of this study therefore, is to quantify historical changes $(1991 - 2019)$ in the floodplain primary producer biomass and freshwater habitats of a large floodplain river in northern Australia (Figs. 1a-c) by integrating Landsat-derived modified normalised difference water index and normalised difference vegetation index in a decision tree framework. The specific objectives of this study are to (i) assess historical dynamics in floodplain inundation in space and time (ii) map the distribution of hot spots of primary producers in freshwater habitats using a classification tree model, and (iii) examine the key hydrological drivers of floodplain productivity and connectivity using multivariate techniques (e.g., Preisendorfer, 1988). Freshwater habitats in most northern Australia catchments are characterised by a wide range of turbidities and spectral properties whose surface becomes cluttered with different aquatic plants after wet season (e.g., Ward et al., 2014; Faggotter et al., 2013). For this reason, most classification algorithms will be restricted in these freshwater systems (e.g., Gidley, 2009)

4

128 for delineating floodplain inundation and primary production centers.

2. Study region

130 The Gilbert catchment in northern Queensland, Australia (Figs. 1a-b) is one of the main
131 river basins of the South gulf region, which has numerous interconnected streams that usually
132 lead to high flows and severe flooding on floodplains. The Gilbert catchment covers an area
133 of 46,200 km^2 and is characterised by strong seasonal rainfall with 93% of rainfall occurring
134 during the summer (Waltham et al., 2013). The catchment is hot and semi-arid with high
135 evaporation rates (1868 mm annual mean) that exceeds rainfall by a factor of 2.4 to 1, and
136 more specifically, 84% of rainfall is lost as evaporation while 13% are converted to streamflow
137 (CSIRO, 2013). The upstream catchment is a high-elevation area (Fig. 1a) characterised by
138 relatively low rainfall, which gradually increases towards the low-elevation areas of the down-
139 stream catchment. Apart from the presence of several river tributaries that receive sufficient
140 groundwater inputs to sustain permanent flows in most freshwater bodies, numerous isolated
141 turbid waterholes that thrives on seasonal rainfall and flow have been identified (e.g., Waltham
142 et al., 2013). These water holes are usually filled by over bank flowing from adjacent rivers
143 during extreme flow events and results in the distribution of aquatic plant biomass (Fig. 1c).
144 Moreover, earlier reports (e.g., Barberm et al., 2013) indicate the water holes provide refugia
145 for a range of fisheries and other aquatic wildlife. The impacts of droughts and extended
146 dry spells have significant influence on the spatial patterns of aquatic plant biomass on the
147 Gilbert floodplain. This is because during such period several of these discreet waterholes and
148 intermittent freshwater bodies usually receive no inflow (Waltham et al., 2013). In addition
149 to ecological values, the agricultural assessment of the Gilbert catchment show that crop pro-
150 duction can reach 60 million /year if crops are grown to full potential (CSIRO, 2013), thus
151 highlighting the economic importance of the region.

3. Data

3.1. Remote sensing data

154 Historical level 1 terrain corrected (L1T) Landsat 5 thematic mapper (TM) and Landsat
155 8 OLI imageries (1991 − 2019) were retrieved from the archives of the United States Geo-
156 logical Survey through an online data portal (https://earthexplorer.usgs.gov/). These
157 imageries, which have temporal resolution of 16 days (i.e., overpass frequencies) and scene
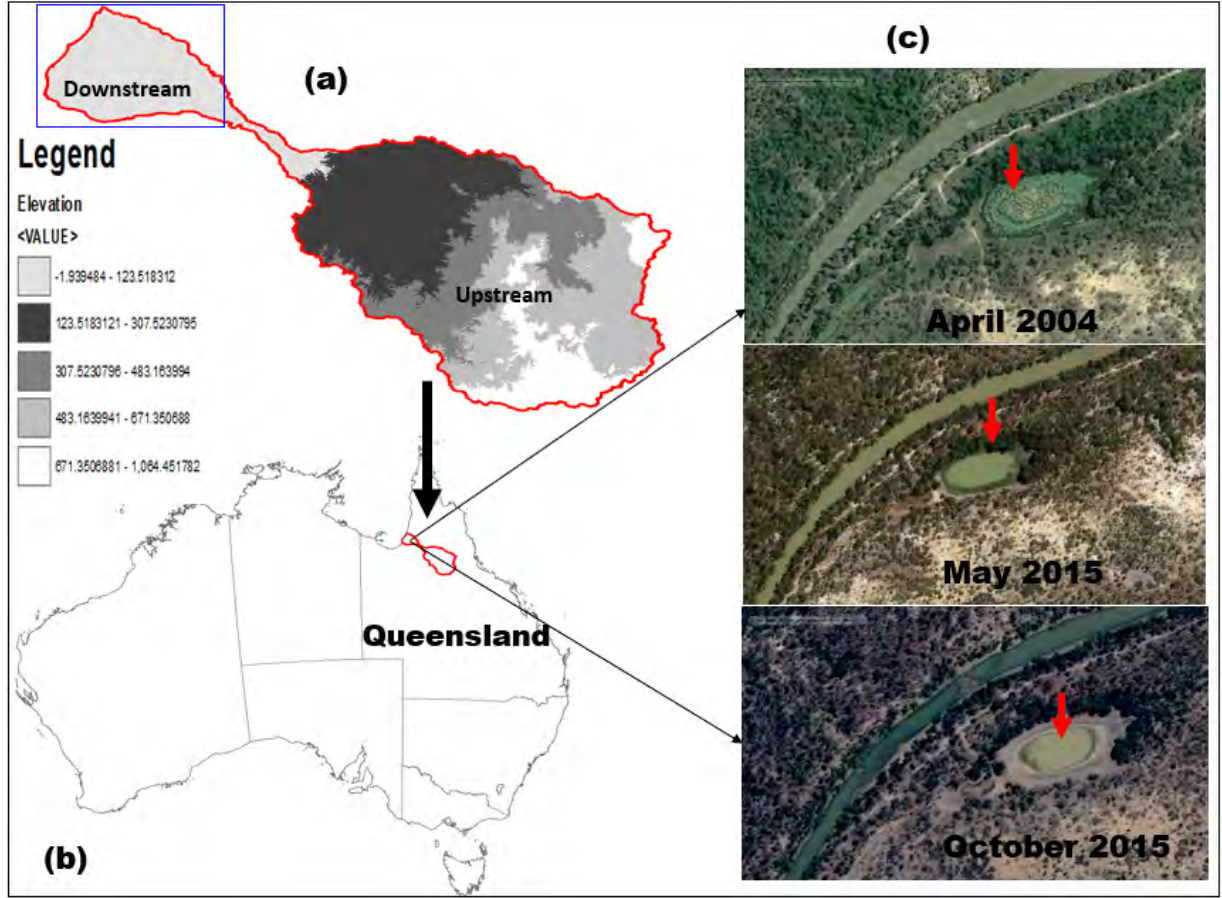
Figure 1: Study region showing the Gilbert catchment in Australia. (a) The Gilbert catchment showing the topographic distribution around the downstream and upstream Gilbert catchment based on corrected digital elevation model, (b) the location of the Gilbert catchment in northern Queensland, Australia and, (c) illustration of the physical dynamics in aquatic primary producer (hot spots) centres under different seasonal conditions in a freshwater habitat (riverine, lacustrine, and palustrine systems) located south-east of the downstream catchment. The red arrow is a typical water hole covered with macrophytes (primary producers) as was the case on the 2nd April 2004. The imageries in (c) were adapted from historical Google-Earth satellite images and World imagery.

quality of nine were retrieved mostly for the wet seasons (January-March) to assess the physical dynamics in freshwater habits and the impacts of hydro-meteorological fluctuation on floodplain productivity during the period. However, few scenes covering the dry seasons of 2009, 2016, and 2018 were also included in the analyses to understand the characteristics of floodplain inundation and primary production centers in extreme wet years and other years. As with several optical systems, the Landsat scenes covering the Gilbert catchments were affected by clouds. So, the imageries with cloud cover greater than 28%, especially those that affected the floodplain corridors (i.e., along the Gilbert river) were excluded while others were

6

preprocessed using a cloud-removal algorithm described in Section 4.1. There were no cloud-free Landsat imageries available for the wet seasons of 2018, so Sentinel-2 image acquired in March, covering most downstream sections of the Gilbert catchment was used to fill that gap. Further details of the satellite imageries used in this study are indicated in Table 1. We noted the years with considerable cloud impacts on wet season satellite images (e.g., 1991, 1998, 2007, 2009).

3.2. Precipitation, river discharge, and stream water levels

The monthly Australian gridded rainfall data used was accessed from the SILOS climate database (https://silo.longpaddock.qld.gov.au/gridded-data). This 8-kilometer monthly rainfall is the accumulated total rainfall over all days in the given month and covers the period between 2000 and 2019. Ground observations of monthly stream water level covering the period $2000-2019$ were obtained from the Queensland Water Monitoring Information Portal (https://water-monitoring.information.qld.gov.au/). The gauged rainfall $(1991-2019)$ observed at downstream Gilbert at Rockfields station (ID-917001D; Lat:-18.2; Long:142.8; Elev:167.7m) was also used to analyse the impact of local precipitation on floodplain productivity. The water level observed at the same station in Rockfield was used in this study as a hydrological indicator to assess the relationship of downstream inundation with averaged satellite precipitation over the entire catchment.

4. Methods

The methodological framework of this study was based on five steps; data acquisition, image preprocessing, classification and segmentation, estimation of floodplain inundation, and prediction of primary production centers (Fig. 2).

4.1. Pre-processing of remote sensing data

The pre-processing involved two main steps; cloud removal and calibration of the raw digital numbers of landsat imageries to surface reflectance. The spectral bands of optical sensors are usually affected by clouds, cloud shadows, and snow, necessitating their identification and removal before use. The influence of cloud varied between 0 and 28% for the Landsat TM and 0 and 12% for the Landsat 8 OLI imageries used in this study (Table 1). To this end, the Fmask algorithm (Zhu et al., 2015) was applied to flag and remove the presence of all clouds and shadows from the multi-band imagery. To calibrate each landsat scene to standard
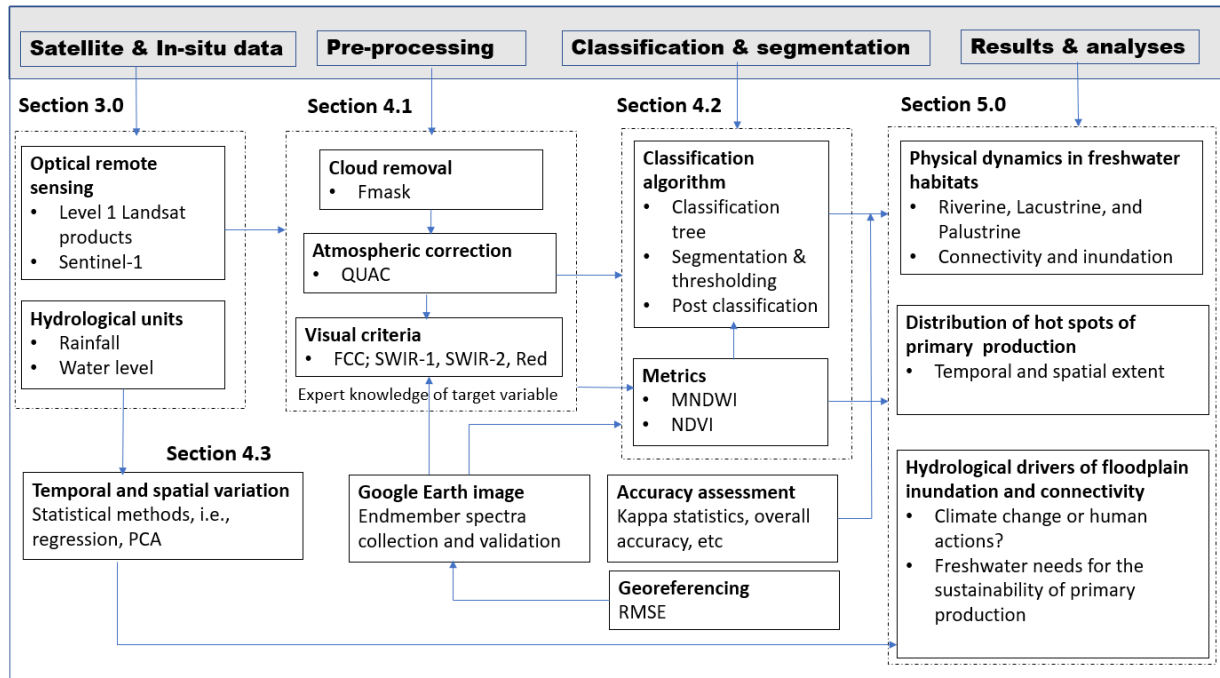
7

Figure 2: Schematic representation of the methodological framework used in this study.

surface reflectance, the QUick Atmospheric Correction Code (QUAC, Bernstein et al., 2005) module in ENVI 5.5 (Exelis Visual Information Solutions) was employed. QUAC performs atmospheric correction on multi-band imageries in a more sophisticated manner (e.g., the use of in-scene approach that relies on information about sensor band locations and their radiometric calibration) and tend to show more merits as opposed to other physics-based methods (see, Bernstein et al., 2005, 2012). Apart from computational efficiency and speed, one key merit of QUAC is its approach to aerosol optical depth retrieval, which does not require the presence of dark pixels (see, Bernstein et al., 2005). The output from QUAC are atmospherically-corrected multi-temporal imageries with similar radiometric scale, regardless of their image acquisition dates, which are usually accompanied by variations in solar irradiance and sensor geometry among other parameters (e.g., Chander et al., 2009). A visual inspection of the False Color Combination (FCC) of these imageries for the target variable (water) in the Gilbert catchment show improved visibility as opposed to other image normalisation approaches and relative atmospheric correction methods (e.g., Song et al., 2001).

4.2. Image classification and segmentation

4.2.1. Floodplain inundation mapping

Based on the expert knowledge of the target variables and field reconnaissance by the project team, visual criteria of the aerial footage was used as a strategic first step to identify the

8

spatial distribution of freshwater bodies in the catchment. This criteria relied on a false colour composition of the red and two infra red bands of landsat data (e.g, Bands 573 for TM) because of the unique spectral property of surface water and its reflectance in these wavelengths. Thereafter, spatio-temporal patterns of floodplain inundation and water bodies were quantified by applying the widely used modified normalised difference water index (MNDWI, Xu, 2006), which combines the green (G) and mid-infra red (MIR) bands as $MNDWI = b_G - b_{MIR}/b_G + b_{MIR}$. There have been several methodological developments around the automated extraction of surface water bodies (e.g., Fisher et al., 2016; Feyisa et al., 2014), which are usually compared against the MNDWI. The latter nonetheless, remains an ideal, mainstream automated water extraction metric because of its accuracy, computational efficiency, and simplicity, especially in threshold identification and definition (ranges from 0-1 for water-related pixels). Supervised and unsupervised algorithms showed limitations because of the diversity in landscapes and the range of turbidities that characterise the Gilbert floodplain rivers and plethora of discrete waterholes. Through segmentation, all waterbodies and inundated areas were extracted and aggregated before estimating their spatial extents.

4.2.2. Identifying hotspots of primary producers

In the characterisation of floating, emergent, and submerged vegetation, it has been argued that rule-based approach such as decision tree could give better results unlike conventional methods (Ozesmi and Bauer, 2002). Consequently, the application of decision trees in the mapping of canopy-forming aquatic vegetation is gradually emerging (Midwood and Chow-Fraser, 2010; Davranche et al., 2010; Zhao et al., 2013). In this study, the distribution of hot spots of primary producers (inundated areas covered with different aquatic species such as macrophytes) in the catchment were mapped by combining the MDNWI and NDVI (normalised difference vegetation index) in a decision tree framework. The spectral properties of the red (R) and near-infred (NIR) bands of landsat, which show relatively low reflectance and high reflectance, respectively were used to estimate NDVI (i.e., $NDVI = b_{NIR} - b_R/b_{NIR} + b_R$) in each of the landsat image. The normalisation of each atmospherically corrected imagery enabled the derivation of catchment-specific quantitative thresholds from NDVI and MNDWI, which were applied in our classification tree model. For instance, the water (e.g., freshwater habitats, floods) isolation phase in this study relied on relied on water-related pixels on the catchment with MNDWI values greater than 0 (Xu, 2006). Whereas the normalisation of calibrated imageries ensures that external factors like water quality difference do not interfere

with the classification stability (e.g., Zhao et al., 2012), several species of floating, emergent, and aquatic plants are known to have mean NDVI values ranging from $0.40 - 0.82$ (Cho et al., 2008). So, the threshold definition for pixels associated with aquatic plants in our classification tree model was NDVI values greater than 0.20. The combination of these thresholds for MNDWI and NDVI in the CT model resulted in the identification of aquatic vegetation within and around freshwater habitats over the Gilbert catchment.

4.2.3. Model validation and accuracy assessment

To minimize the need for field campaigns and validation whilst making it an accurate general-purpose application suitable for other floodplain wetlands, our classification tree model is compared to a physically-based spectral classification algorithm (Kruse et al., 1993) as summarised in Fig. 2. The output from the classification tree (CT) was compared with spectral angle mapper (SAM), a pixel-based classification algorithm that depends on the spectral similarity between two spectra (Kruse et al., 1993). So, to assess the efficacy of physically-based spectral classification algorithm, several endmember spectra (i.e., spectral profiles) in the catchment were collected from hot spots of primary production and freshwater bodies using the Google Earth image as a reference. The classification of hot spots and inundation from the SAM (ten different endmember spectra were collected) and CT model based on the April 2005 landsat data were subsequently compared with pure pixel validation data from Google Earth imageries. Notably, image-to-image co-registration of Google Earth imagery and landsat image (23rd April, 2005) based on several control points was employed for the validation sites. The geo-referenced Google Earth data was then used as reference map for accuracy assessment based on kappa statistics (e.g., Congalton and Green, 2009).

4.3. Multivariate analysis of hydrological indicators

– *Identifying dominant patterns of rainfall*

The multivariate analyses of rainfall over the Gilbert catchment was achieved with the use of principal component analysis (PCA, Preisendorfer, 1988). The Bartlett's test statistics (Snedecor and Cochran, 1989) was first employed to identify the statistically significant orthogonal modes of rainfall variability over the catchment. The rainfall grids were masked over the Gilbert catchment and statistically decomposed using the PCA technique. Consider a centered matrix of rainfall grids (i.e., after removing the mean) masked over the Gilbert catchment as $\mathbf{X} = [x(p_k, t)]$ where p_k is spatial locations; k = 1,

10

$_{277}$ 2, . . ., nx, which are the number of spatial locations for $\mathbf{X}$, and t is the monthly time

$_{278}$ step from $2000 - 2019$. The statistical decomposition of rainfall grids into spatial and

$_{279}$ temporal patterns using this method is given as (e.g., Ndehedehe et al., 2019a),

$$\mathbf{X}(t) = \sum_{k=1}^{n} a_{(k)} \mathbf{p}_k \tag{1}$$

$_{280}$ where $a_{(k)}(t)$ are the temporal variations also called expansion coefficients (or sometimes

$_{281}$ standardised scores) and $\mathbf{p}_k$ are the corresponding spatial maps (empirical orthogonal

$_{282}$ functions-EOF loadings). The dominant orthogonal modes of rainfall (a combination of

$_{283}$ the temporal and spatial patterns) are the first few pairs obtained from the PCA method.

$_{284}$ Each principal component represents a fraction of the total variation that is proportional

$_{285}$ to the amount of covariance in time explained by each eigenvector (spatial loadings). The

$_{286}$ total variance accounted for by each orthogonal mode was computed similar to previous

$_{287}$ studies (e.g., Ndehedehe et al., 2019a). By reducing the number of orthogonal modes,

$_{288}$ the dominant patterns of rainfall variability associated with floodplain productivity in

$_{289}$ the catchment were identified.

$_{290}$ – *Cross-correlograms, regression, and estimation of mutual information*

$_{291}$ Cross-correlograms were employed to examine the relationship and similarity between

$_{292}$ hydrological indicators (rainfall, river discharge, and water level) and floodplain produc-

$_{293}$ tivity whilst also estimating their corresponding lags (i.e., the number of time periods

$_{294}$ that separate the two variables). In addition to the use of linear regression to assess

$_{295}$ relationships, Mutual Information (MI) criteria (e.g., Moon et al., 1995; Sharma, 2000)

$_{296}$ was employed as a more reliable measure of statistical dependence between two variables

$_{297}$ because of its merits over other statistical measures that rely on residual sum of squares.

$_{298}$ Whereas MI is useful in understanding the dependence between two time series that

$_{299}$ appear to be related or independent, one key advantage of this technique is that it mea-

$_{300}$ sures more than linear dependence (e.g., Brillinger, 2004; Moon et al., 1995). This could

$_{301}$ be the case with either rainfall or flow with aquatic primary production in the Gilbert

$_{302}$ catchment, hence the suitability of the MI criteria. If a set of two variables (e.g., river

$_{303}$ discharge and hot spots) are denoted as $X = x_1, x_2, x_3, ..., x_n$ and $Y = y_1, y_2, y_3, ..., y_n$

$_{304}$ where n is the sampling length, the MI between these variables for the non-parametric

$_{305}$ case is defined as (e.g., Brillinger, 2004; Moon et al., 1995),

$$MI_{x,y} = \int \int k(x,y) p(x,y) \log \frac{p(x,y)}{pX(x)pY(y)} dxdy, \tag{2}$$

11

Table 1: Summary of the remote sensing data used in this study to generate inundation and vegetation metrics used in the classification tree.

Data	Sensor	Resolution			cloud coverage (%)	Period	Data type	Swath width (km).	Paths/Rows	Providers
		Spatial (m)	Temporal (days)	Spectral (bands)						
Landsat 5	TM	30	16	7	0-28	1991-2010	Level 1 TP	180	98/72	USGS
Landsat 8	OLI & TIRS	30	16	11	0-12	2014-2019	Level 1TP	180	98/72	USGS
Sentinel-1	S2A & S2B	10, 20, 60	5-10	13	0.1	2018	Level 1C	290		ESA

Table 2: Summary of accuracy assessment parameters (overall accuracy, kappa coefficients, commission and omission errors) for open surface water mapping and prediction of hot spots of primary production in the two reference sites at the Gilbert catchment using NDVI and MNDWI in classification tree framework.

Reference location	Overall accuracy (%)	Kappa (%)	Producers accuracy (%)		User accuracy (%)		Omission error (%)		Commission error (%)	
			Open water	Hot spot	Open water	Hot spot	Open water	Hot spots	Open water	Hot spots
Site 1	94.50	89.10	95.24	93.55	100.00	93.55	4.70	6.50	0.00	6.50
Site 2	94.60	74.0	97.01	75.00	98.48	100.00	2.99	25.0	1.52	0.00

where $p(x, y)$ is the probability density function and k is a kernel function that is aimed at improving asymptotic properties (e.g., Brillinger, 2004). The kernel density function that was plugged into Eqn. 2 is the multivariate Gaussian probability density function and follows the formulation in Moon et al. (1995). For comparability, the MI for bivariate samples (e.g., rainfall vs inundation and discharge vs extent of aquatic primary production, etc.) were scaled similar to cross-correlation coefficients.

5. Results

5.1. Classification trees versus endmember spectra collections

The classification tree (CT) model extracted 95353 pixels (0.97%) as hot spots of primary production and 51279 pixels (0.52%) as open water in the validation image used. The endmember spectra profiles (Figs. 3a and b) used in the SAM algorithm of the same validation image resulted in the classification of 37902 pixels as hot spots of primary production while 20894 pixels were extracted as open water. From the visual assessment of spatial patterns (Figs. 3c and f) and the separability of freshwater habitats (i.e., for riverine and lacustrine systems) and hot spots of primary production (Figs. 3d and i), the CT model performed better than the SAM algorithm. For instance, the river systems extracted by our CT model are uniform and well connected (Fig. 3d) as opposed to the SAM model, which appear to be patchy and sketchy with several disconnections along the river channel (Fig. 3g). Within the same river system or water channels, be it inland or coastal waters, there is a significant difference in the
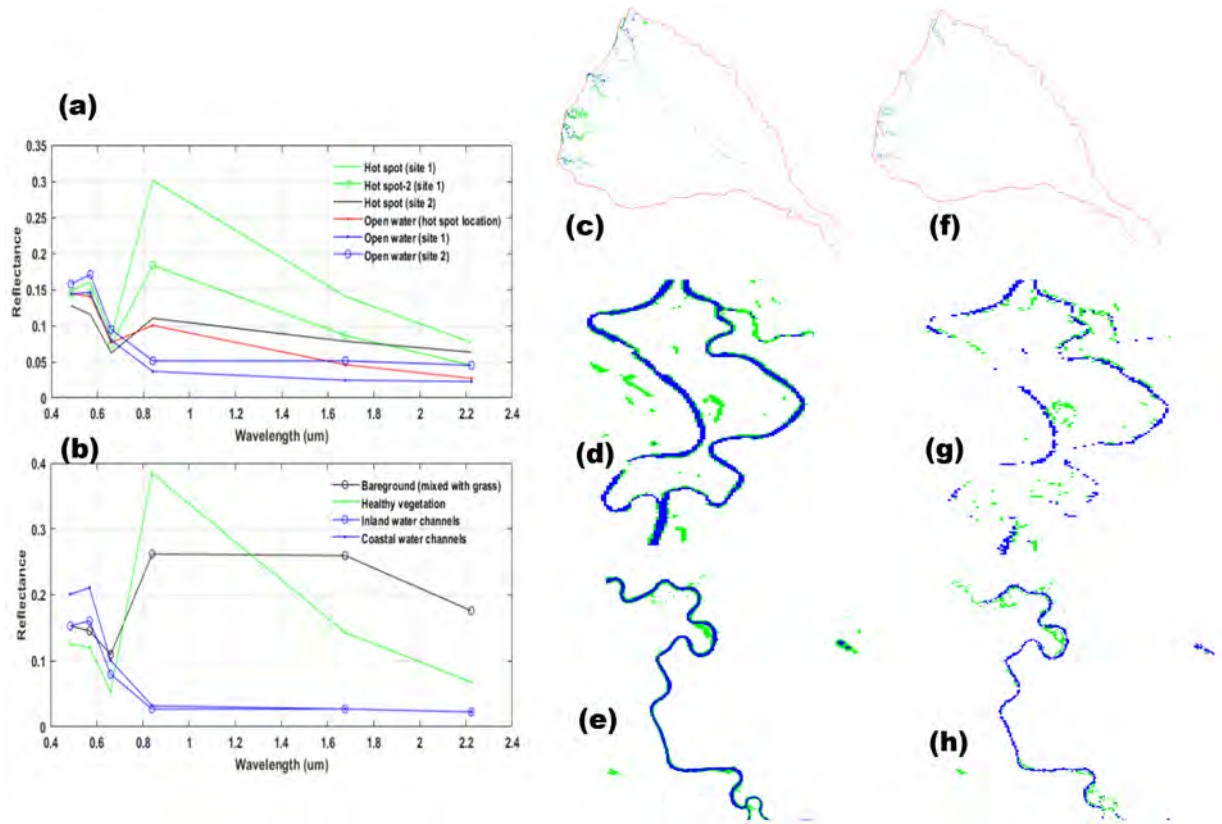
Figure 3: Separability of freshwater habitats and hot spots of primary production. (a-b) Spectral profiles for land cover states associated with aquatic ecosystems and water bodies with a range of spectral properties in the Gilbert catchment, including the two reference locations. These endmember spectra (signature profiles) were collected from calibrated Landsat imagery (21st April 2005) for the reference locations and other randomly selected sites (include areas near the coast) and used in the Spectral Angle Mapper supervised algorithm. (c-e) and (f-h) are raster maps from classification tree and endmember collections of freshwater habitats (blue) and hot spots of primary production (green), respectively.

physical properties of water (Figs. 3a and b), making the use of SAM algorithm in large-scale floodplain productivity mapping more complex and challenging. To improve the performance of SAM in Figs. 3g and h, this would require rigourous collection of numerous endmember spectra in the Gilbert catchment. But the rule-based approach simplifies the classification of these freshwater ecosystems. A further validation step for the CT model used for the mapping of floodplain inundation and hot spots was achieved using the Google Earth image of the same month as the landsat TM image. Based on a first-order polynomial transformation, the geo-referenced accuracy of the referenced data showed RMSEs of 0.013 and 1.24 for the first and second spatial locations, respectively. Differences encountered in the process of image-to-map registration before kappa analysis can contribute to the overall accuracies and kappa coefficients. The latter is relatively lower in the second location (74%) compared to the first
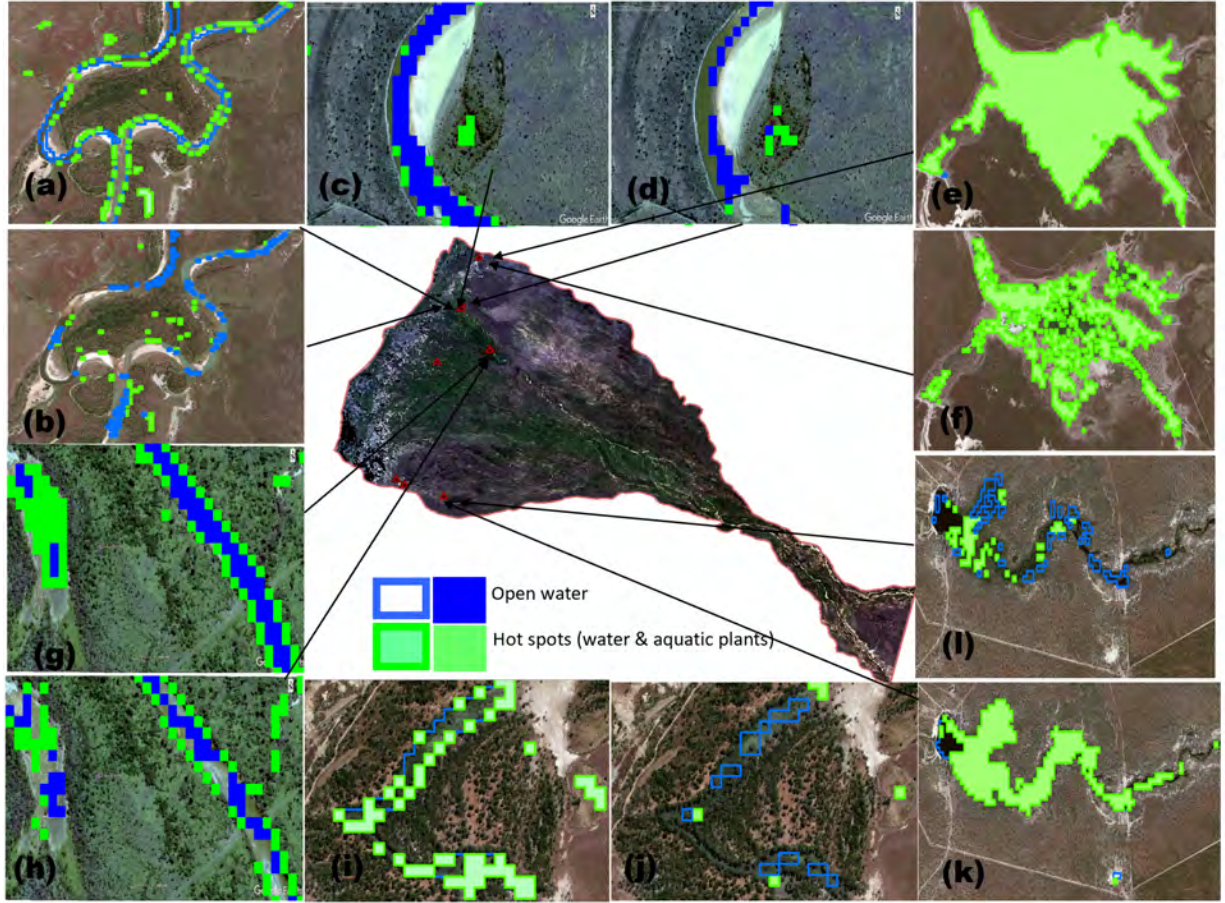
Figure 4: Efficacy of classification tree framework in assessing floodplain inundation and mapping freshwater habitats in the Gilbert catchment. The vectorized polygons in (a), (c), (e), (g), (i), and (k) were derived from the combination of NDVI and MNDWI in a classification tree while (b), (d), (f), (h), (j), and (l) are spectral angle mapper classification using a range of endmeber spectra collection. The pairs (a)/(b), (e/f), (i/j) are some illustrations highlighting the performance of classification tree and spectral g mapper for Riverine, Lacustrine, and Palustrine systems, respectively. Satellite imageries in (c-d) and (g-h) are from Google Earth while others are 0.5 m spatial resolution World View-2 data archived by Digital Globe and were captured in April 2015.

location with kappa value of 89.1% (Table 2). While the geo-referenced accuracy of the referenced image in the second location may contribute to this kappa value and the entire error matrix as already echoed in the literature (e.g., Congalton and Green, 2009), generally the kappa statistics, including all assessment parameters indicate that the CT model performed considerably well (Table 2). The efficacy of the CT framework over the SAM algorithm in assessing floodplain productivity is further illustrated for other freshwater habitats using the post processed classification outputs, i.e., vectorized layers overlayed on referenced imageries and 0.4 m World imagery (Figs. 4a-l). The extracted Lacustrine (Figs. 4e and f) and Palustrine (Figs. 4i and j) systems from both methods show significant differences with SAM showing

14

³⁴⁵ some patches and disconnections as earlier highlighted contrary to the CT model. These same
³⁴⁶ attributes are also evident in the zoomed-in floodplain rivers and predicted hotspots of primary
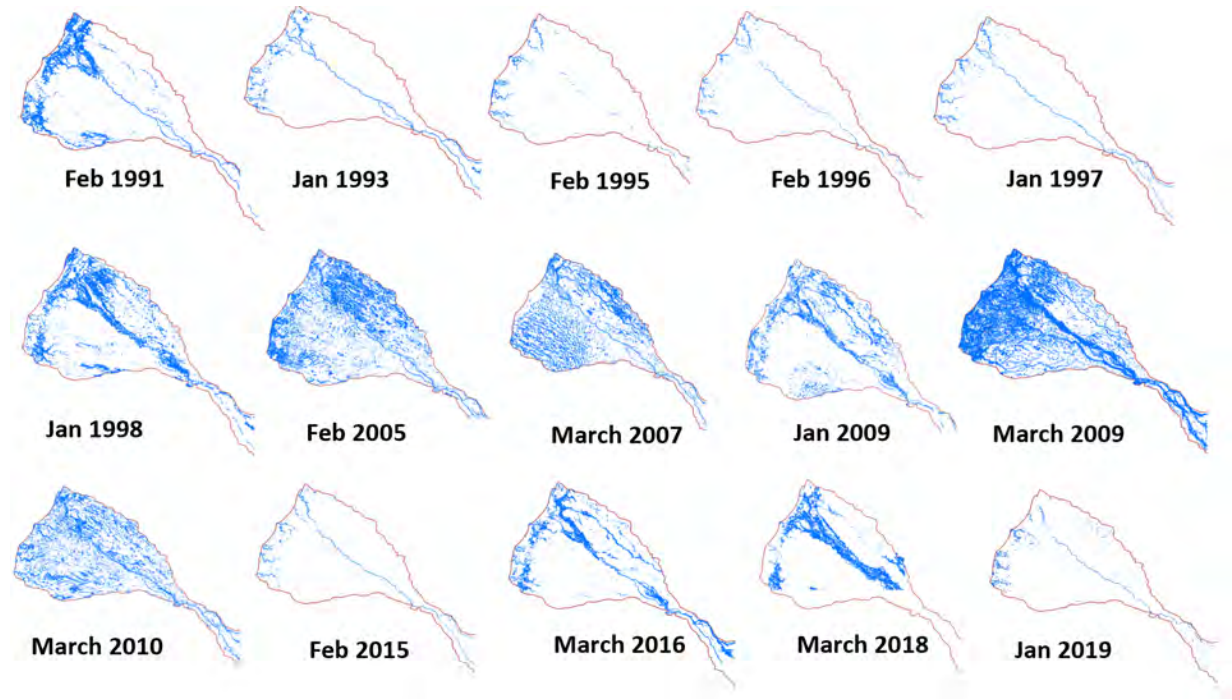production (Figs. 4c-d and g-h).

Figure 5: Spatial patterns of Landsat-derived wet season (January, February and March) floodplain inundation over the Gilbert catchment for selected years based on the MNDWI. Owing to the lack of cloud-free Landsat data for wet season in 2018, available cloud-free Sentinel 1 data covering most segments of downstream Gilbert catchment was used to estimate inundation for March 2018.
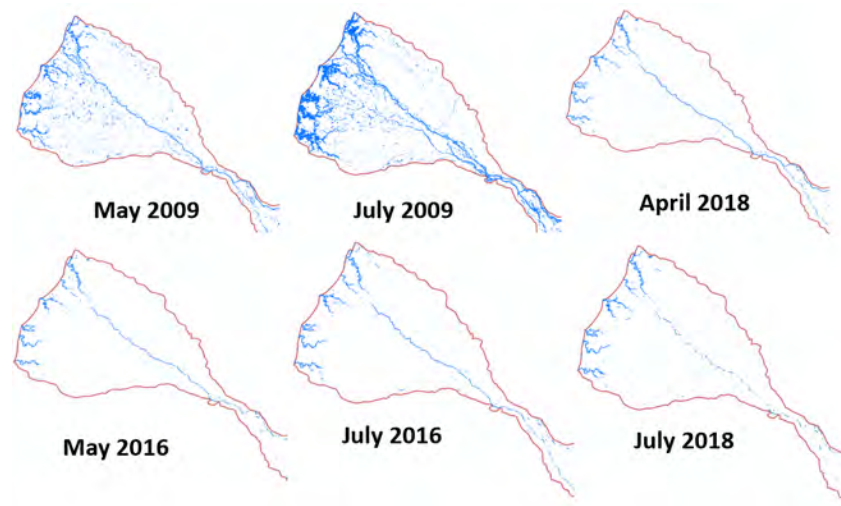

Figure 6: Comparing floodplain inundation during dry season (e.g., April, May and July) for years with high magnitude flood events and relatively dry periods.

³⁴⁷

15

Table 3: Association of local rainfall and observed discharge at downstream Gilbert with estimated extents of hot spots (HS) of primary production and inundation (Inund) using Mutual Information criterion and maximum (max) correlation. The relationship between HS and inundation extent is also indicated.

Criteria	Rainfall vs HS	Rainfall vs Inund	Flow (mean) vs HS	Flow (max) vs HS	Flow (mean) vs Inund	Flow (max) vs Inund	HS vs Inund
Mutual Information	0.46	0.57	0.32	0.36	0.56	0.55	0.87
Correlation (max)	0.57	0.71	0.68	0.65	0.61	0.66	0.83

5.2. Floodplain inundation and hotspots of primary production

5.2.1. Floodplain dynamics and seasonal inundation

The spatial patterns of inter-annual floodplain inundation during wet season over the downstream Gilbert catchment showed marked differences (Fig. 5). From the historical cloud-free imageries retrieved from the landsat archives, the period between 1998 and 2010 are the wettest since 1991 while the years between 1993 and 1997 were relatively dry (Fig. 5, cf. Fig. 7). The magnitude of the 1998 flood event was a considerable deviation from this previous dry periods or spells (excluding 1991) and led to about 1144 km^2 inundation extent. However, the hydrological records (discharge and water levels) of the downstream Gilbert catchment indicate 2009 has been the wettest year in more than two decades. Although about 26% of the January 2009 landsat imagery was affected by cloud (mostly around floodplains), inundation extent recovered within the main floodplain along the Gilbert river was about 708 km^2. The floodplain remained highly productive in March 2009, resulting in an inundation extent of approximately 940 km^2. Moreover, it seems the impacts of extreme wet season flood have considerable influence on the floodplain productivity of dry season within the same year. For example, comparing the floodplain inundation in May and July of 2009 and 2016, years with different levels of flood magnitude, 2009 was relatively more productive even in dry season unlike 2016 (Fig. 6). Similarly, April and July 2018 inundation was not very different given that the wet season of the same year was relatively wetter than 2016 (Fig. 6). Except for the $2016 - 2018$ period (though rather wet, there was no cloud-free image for 2017 wet season), $2014 - 2019$ is generally much similar to the dry cycles of the mid-1990s with 2015 being the driest (26.7 km^2) (Fig. 5, cf. Fig. 7).

Rainfall seasonality is a critical indicator of the spatial distribution of floodplain inundation in the Gilbert downstream catchment. For example, floodplain inundation extent as at 31st of March 2009 was approximately 940 km^2. By 21st July of the same year when there is usually little or no rainfall, estimated inundation extent was 108 km^2 (Fig. 6). Similarly, about 326 km^2 spatial inundation extent was estimated on 18th March 2016. This inundation

extent receded to approximately 25 km^2 by 24th July 2016. Notably, the change in seasonal floodplain inundation have impact on the distribution of primary producers both in the wet and dry seasons (Figs. 6-8). For example, the predicted extent of primary production reduced from 25 km^2 in early April 2018 to about 3 km^2 in mid-July of 2018. The spread of hot spots of primary producers were also revealed in their transitional patterns during wet seasons. In 2009 for instance, hot spot extent was about 44 km^2 as at January 26th (though this month's imagery was significantly affected by cloud) because of the heavy flood and standing water on the floodplain. By 31st March, 2009 rainfall and discharge had reduced significantly, resulting in extensive evolutions of hot spots of primary production (859 km^2) (Fig. 7). These same patterns were observed in other imageries, including those of 2010 (13th January-265 km^2; 18th March-454 km^2), 2016 (14th January-4 km^2; 18th March-79 km^2), and 2019 when the estimated extents of hot spots rose from about 5 km^2 in January to about 11 km^2 in mid-March.
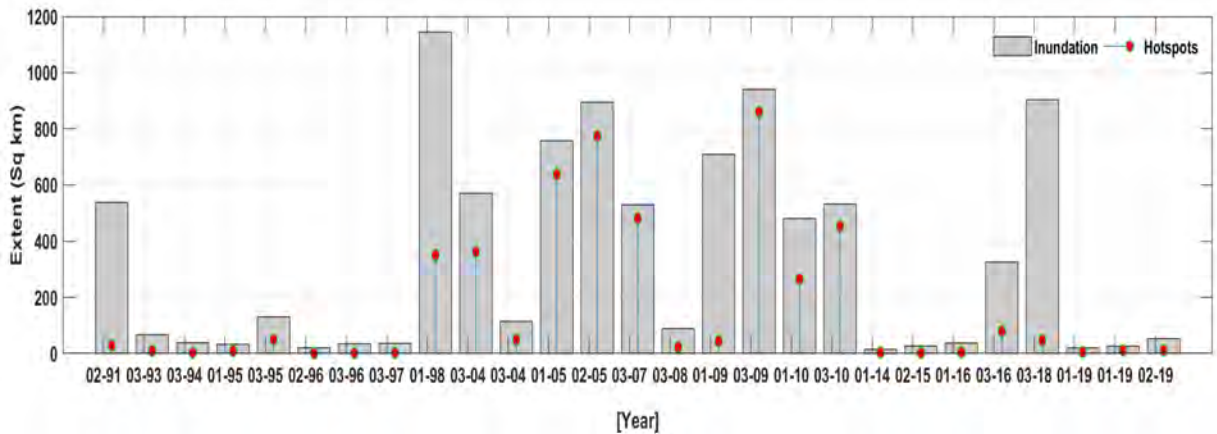

Figure 7: Historical patterns of wet season floodplain inundation and predicted hot spots of primary production derived from a combination of NDVI and MNDWI. These vegetation and inundation metrics were employed in a decision tree framework to estimate hot spots of primary production and aquatic ecosystems.

5.2.2. Spatial and temporal distribution of floodplain productivity

The temporal patterns of the predicted hot spots of primary producers for the $1991 - 2019$ period are embedded in Fig. 7. Except for overwhelming flood periods (e.g., February 1991, January 1998, January 2009, and March 2018), these patterns show that there is a reasonable agreement between floodplain inundation and the evolution of primary production ($r = 0.73$). While mutual information (MI) and maximum correlation between extents in hot spots of primary production and inundation are considerably higher ($r = 0.83$ and $MI = 0.87$,
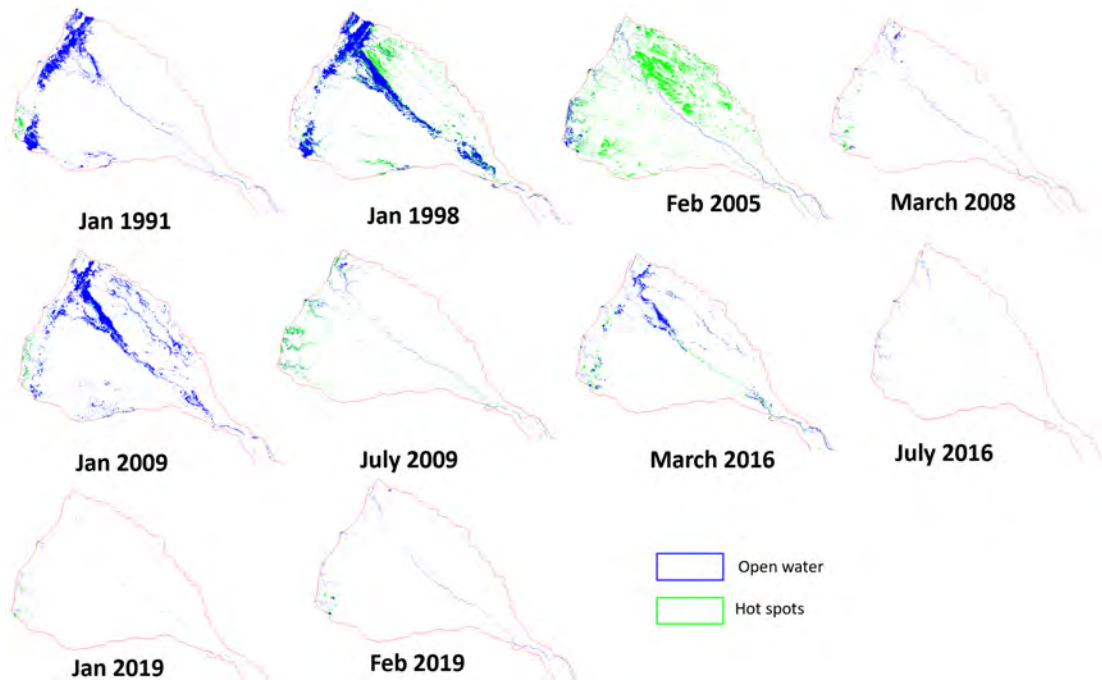
17

Figure 8: Raster maps showing spatial patterns of hot spots of primary production for years with flood events and relatively dry years.

respectively) with a phase lag less than one month, the distribution of hot spots show spatial heterogeneity over the Gilbert catchment (Fig. 8). Spatially, the year 2019 show less primary production with spatial extents of approximately 11 km^2 each in the months of January and February unlike 2005 (Figs. 8, cf. Fig. 7). However, the drought in 2015 affected productivity on the floodplain and showed the lowest extent (about 2 km^2) since 1997, i.e., based on the available imageries (Fig. 7). Spatial patterns of productivity (Fig. 8) in dry seasons of extreme wet years (e.g., July 2009) are significantly different from dry seasons of moderately wet years (e.g., July 2016).

On a more localised scale, the influence of floodplain inundation and impacts on the spatial patterns of aquatic habitats, especially water holes and primary production centers are indicated (Figs. 9a-j). The biomass accumulation of aquatic canopy-covering plants in water holes (Fig. 9a) and the persistence of similar freshwater habitats depend on over bank spilling of floodplain rivers into these freshwater domains during extreme or severe wet periods (Figs. 9d, f-g, and i). The connectivity of these rivers with slightly isolated water holes and other intermittent water bodies can last up to 4 months and more during such extreme wet periods (Figs. 9f-g). At the start of the wet season, they exist independently and get connected as the wet season progresses or depending on the intensity and magnitude of flood (Figs. 9c-d and h-

18

i), and later disconnect at the end of the wet season (Fig. 9e). Note that Fig. 9j does not imply the disappearance of the floodplain river but rather implies a contraction of the river beyond what the 30 m pixel size of landsat can capture. This contraction could be caused by change in precipitation patterns, which in turn influence flow variability and subsequently floodplain inundation patterns. Further, the spatial patterns of floodplains in the riverine systems towards
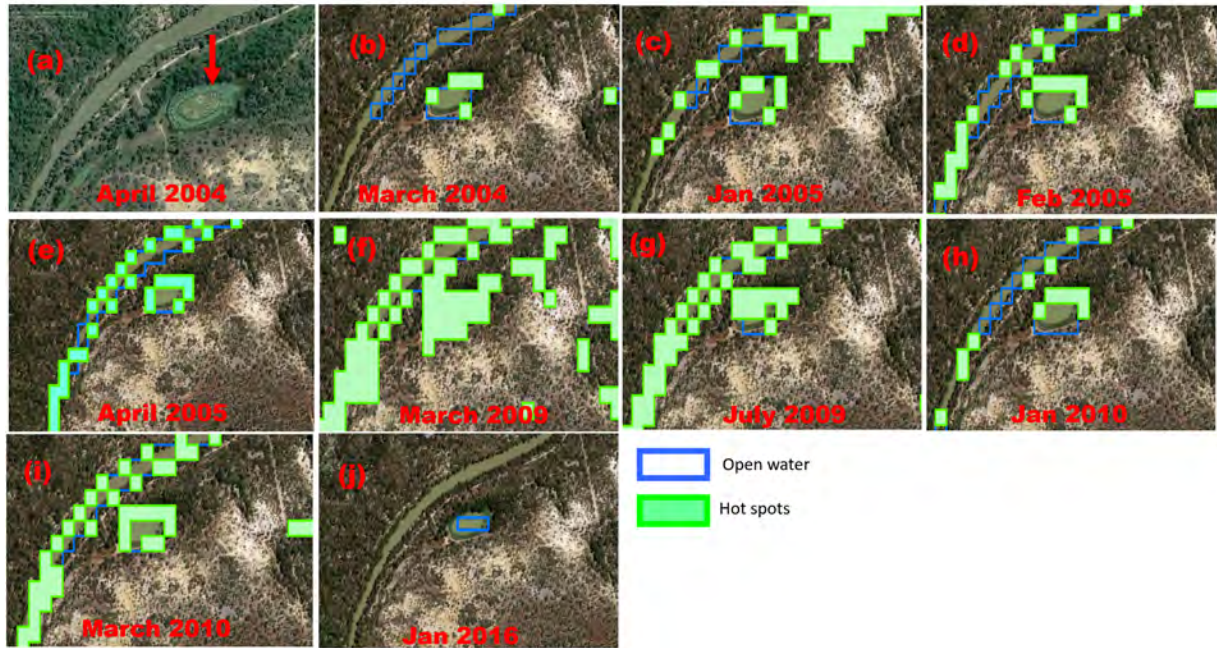

Figure 9: Seasonal floodplain inundation and impacts on the physical dynamics of aquatic habitats and primary production centers. (a) Freshwater habitats showing intermittent floodplain water bodies in downstream Gilbert catchment (red arrow is a typical water hole covered with macrophytes-hot spot of primary production). (b-j) indicate the changing patterns of inundation and primary production in these freshwater habitats. The high-resolution satellite imagery in (a) is taken from Google Earth and was captured in April 2004 while others were taken in May 2015.

the end of wet season (March ending) also show interesting patterns (Figs. 10a-j). As the dry season approaches, some tributaries of the Gilbert river remain disconnected in relatively dry years with no significant floods (Fig. 10a-c) while the riverine systems in wet years remain connected with some wet years having excessive flood waters along the floodplain rivers as was the case in 2009 and 2018 (Fig. 10d, g, and i-j).

5.3. Impacts of rainfall variability on floodplain productivity

The downstream monthly total rainfall and river discharge did not appear to be directly related with the estimated extent of hot spots of primary producers (Figs. 11a-c) unlike floodplain inundation (Figs. 11d-e). However, from the cross-correlograms and mutual information
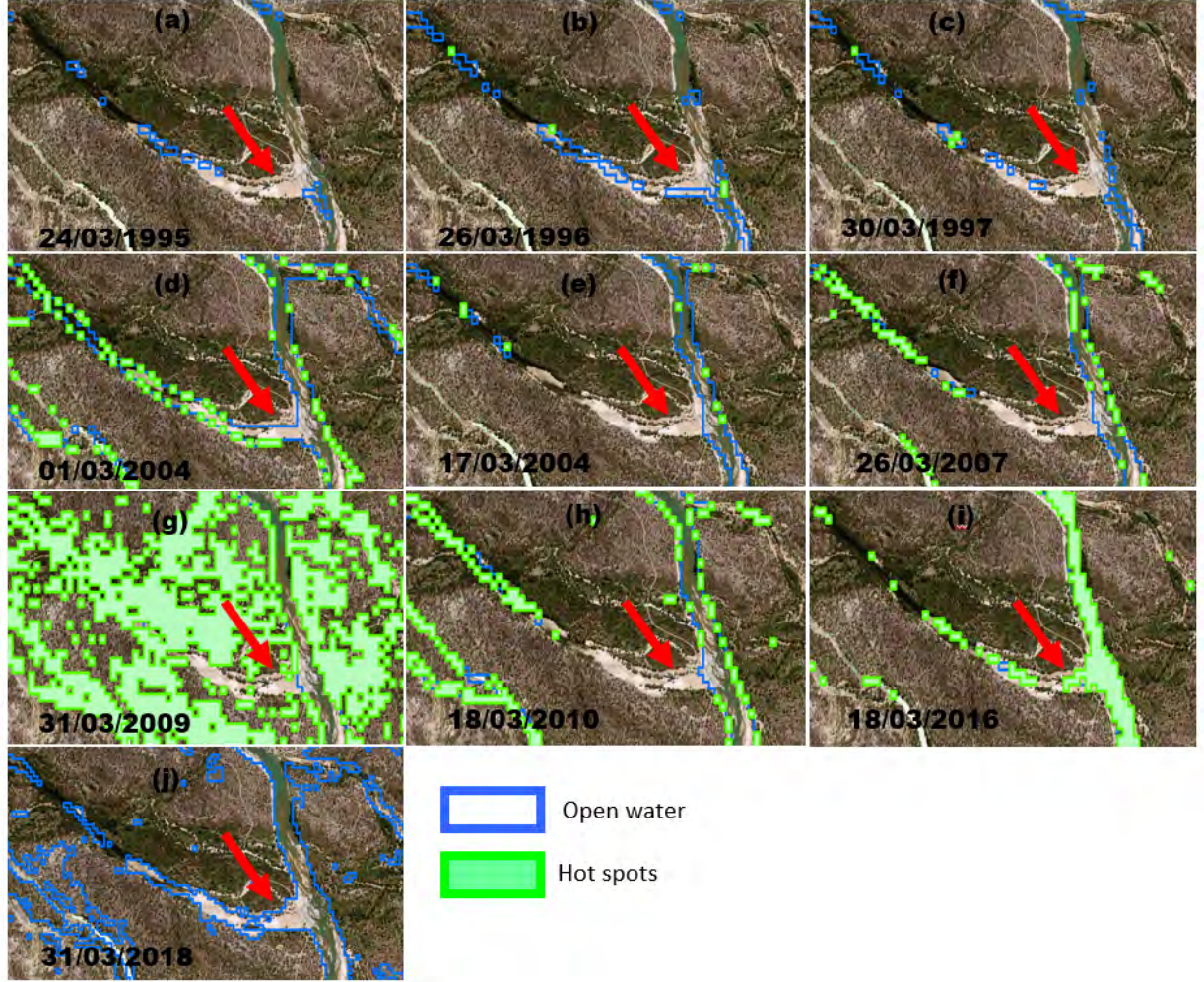
Figure 10: Illustration of the spatial dynamics of floodplains in the riverine systems towards the end of wet seasons using available Landsat imageries. (a)-(j) show the inundation patterns (temporal and spatial) of the lower Gilbert river located downstream and their connectivity to the tributaries in March ending.

(Table 3), rainfall was moderately associated with predicted extents of primary production (Figs. 11 g and j), indicating peak correlation of 0.57 at three months phase lag while the rainfall-floodplain inundation relationship shows a maximum correlation of 0.71 at zero phase lag. Although a cause and effect relationship is expected, preceding rainfall in the downstream or upstream (conveyed through discharge) catchment drives the productivity of the catchment. In this regard, similar to rainfall, we also found a linear relationship between discharge and floodplain inundation (Figs. 11e) but not with hot spots. That is, correlation (r) of hot spots with rainfall ($r = -0.21$) and mean discharge ($r = -0.13$) are negative, suggesting poor associations contrary to the rainfall-inundation ($r = 0.36$) and discharge-inundation relationships ($r = 0.39$). However, the mean and maximum river discharge observations of the downstream catchment showed linear associations (maximum correlations $r = 0.61$ and $r = 0.66$, respec-
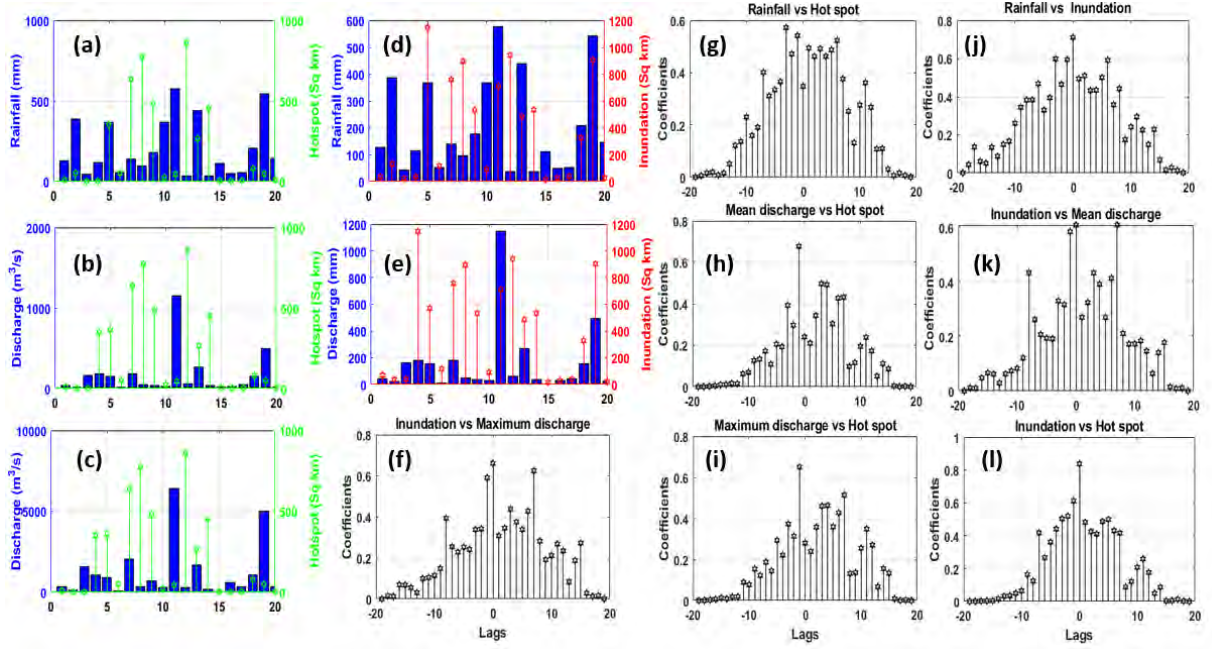
Figure 11: Correlation of downstream wet season rainfall (monthly totals) and flow with floodplain productivity during the 1995 − 2019 period. The relationship of total monthly rainfall amounts with predicted extents of hot spots of primary producers and total inundation extent are indicated in (a)-(e). (f-k) Are their corresponding cross-correlograms during the same period with lags indicated in months. (f and i) Are the cross-correlograms of observed maximum discharge at downstream catchment with floodplain inundation and hot spot while (l) is the cross-correlogram between floodplain inundation and hot spot. Periods corresponding to Fig. 7 with missing total rainfall amounts (30/03/1997, 1/03/2004, 06/01/2019, and 23/02/2019) and discharge have been excluded in the analyses.

tively) with floodplain inundation extent at phase lags less than one month and (Figs. 11k and f). As opposed to rainfall, relatively higher peak correlations between discharge ($r = 0.68$ and $r = 0.65$ for mean and maximum discharge observations, respectively) and hot spots of primary production were observed and indicated one month phase lag (Figs. 11h and i). Apparently, the maximum observed association between rainfall and hot spots is relatively lower than the discharge-hot spots relationship. While other biophysical factors could promote growth of aquatic primary producers, it is also obvious that the spread of hot spots is strongly tied to the presence of water on the floodplain (Fig. 11l). The relationship of estimated extents of aquatic primary production with local rainfall and discharge at downstream Gilbert as identified using the mutual information criteria (Table 3) further confirm that rainfall and discharge are key optimal predictors of floodplain productivity.

There are two orthogonal modes of rainfall in the Gilbert catchment that drives the variability in floodplain inundation. The first mode highlights the changes in annual rainfall and
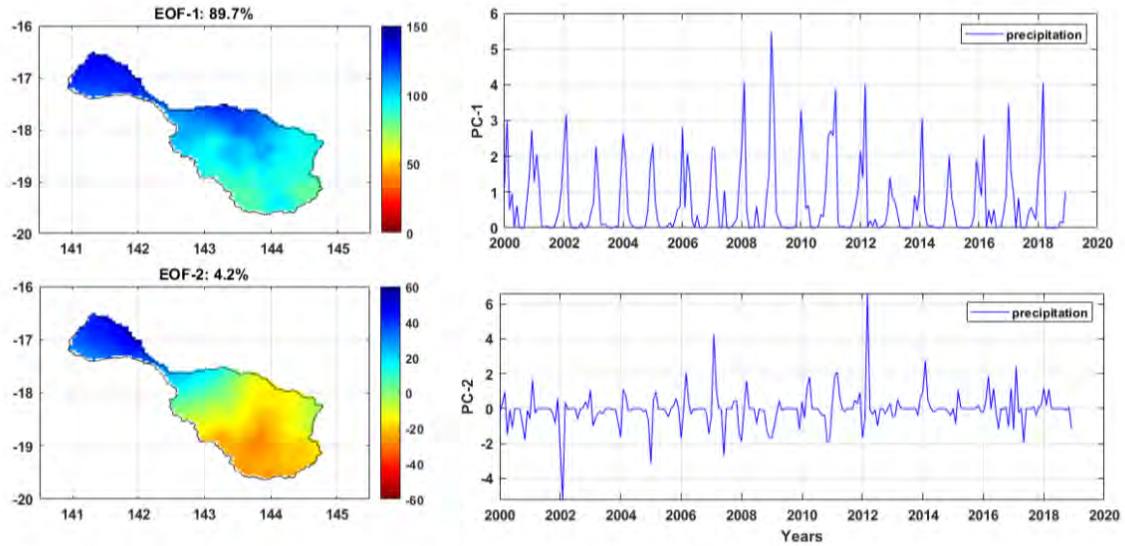
21

Figure 12: Spatio-temporal rainfall variability over the Gilbert catchment (2000 − 2019). The EOFs (left) are loadings showing spatial patterns of precipitation (mm) while the corresponding principal components (right) are temporal variations, which are normalised using their standard deviation to be unitless. Averaged monthly rainfall values over each grid in the catchment are jointly derived from the principal components and spatial loadings (maps). The variances (in percentages) accounted for by each orthogonal mode are also indicated.

accounts for approximately 90% of the total variability while the second mode is a short term seasonal signal that accounts for about 4% of the total variability (Fig. 12). The leading rainfall mode observed over Gilbert has strong EOF loadings in downstream Gilbert (EOF-1, Fig. 12). The corresponding temporal patterns (PC-1, Fig. 12) associated with spatial patterns indicate 2009 had the highest amount of annual rainfall and sufficiently explains the inter-annual variability of floodplain inundation in this downstream catchment. These rainfall amounts were very consistent with the stream water levels and discharge (maximum discharge recorded was more than 6300 m^3/s) of the downstream Gilbert (Supporting information, S1). However, the short term fluctuations in rainfall (EOF-2/PC-2, Fig. 12) contribute significantly to the seasonal variability in floodplain productivity. For the downstream catchment (cf. Fig. 1a) such years include, e.g., 2007, 2012, 2014, 2017 while the upstream catchments had marked fluctuations, e.g., in 2002, 2005, and 2007 (PC-2, Fig. 12). The increased alimentation of the floodplain and the connectivity of freshwater habits are somewhat sustained by these short term seasonal rainfall variations.

Overall, averaged rainfall over the Gilbert catchment show significant associations with observed water level variations at the downstream region (Fig. 13). Be it averaged wet season rainfall or monthly rainfall deviations (after removing the mean), its association with

monthly wet season water level ($r = 0.83$) or maximum monthly water level ($r = 0.87$) at the downstream catchment is considerably high and significant (Fig. 13a-b). Even the monthly departures (Fig. 13c) of averaged wet season Gilbert rainfall is strongly associated with wet season stream water levels ($r = 0.96$). Moreover, the leading rainfall mode over Gilbert catchment (PC-1, Fig. 12) explained a significant high proportion of observed discharge ($r = 0.83$) (Fig. 13d), confirming the contributions of high elevation upstream catchment (cf. Fig. 1a) to downstream floodplain productivity. For example, except for 2002, which was not analysed, the period between 2007 and 2013 show strong deviations in water levels, rainfall, and discharge (Fig. 13a-b) and coincides with periods with increased floodplain inundation extent and evolution of hot spots of primary production (Fig. 7). Indeed, hydrological changes have influence on the seasonal and inter-annual characteristics of floodplain inundation, which in turn impacts the connectivity of freshwater habitats (Figs. 14a-i).
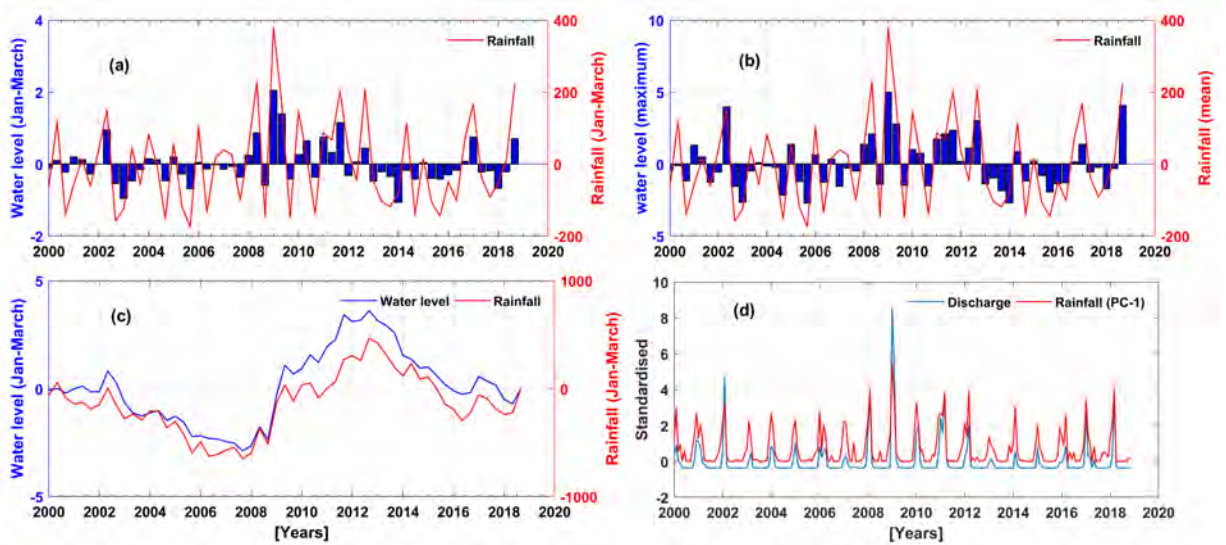

Figure 13: Relationship between averaged rainfall masked over the Gilbert catchment and stream water levels during the 2000-2019 period. (a) Monthly anomalies (i.e., after removing the mean) in observed mean values of stream water level and averaged rainfall over the Gilbert for the wet seasons (January-March) only. (b) Deviations in monthly (all time steps) maximum water level and rainfall, (c) cumulative departures of wet season rainfall and water level, and (d) relationship between leading rainfall mode (PC-1, Fig. 12) over the entire Gilbert and observed discharge downstream Gilbert catchment.

6. Discussion

6.1. Spectral separability and optical differences of aquatic habitats in wet-dry tropics

The properties of water can be affected by algal blooms, tidal cycles, sediment inputs and reflectance from depth and bottom (e.g., Fisher et al., 2016; Tulbure et al., 2016). While
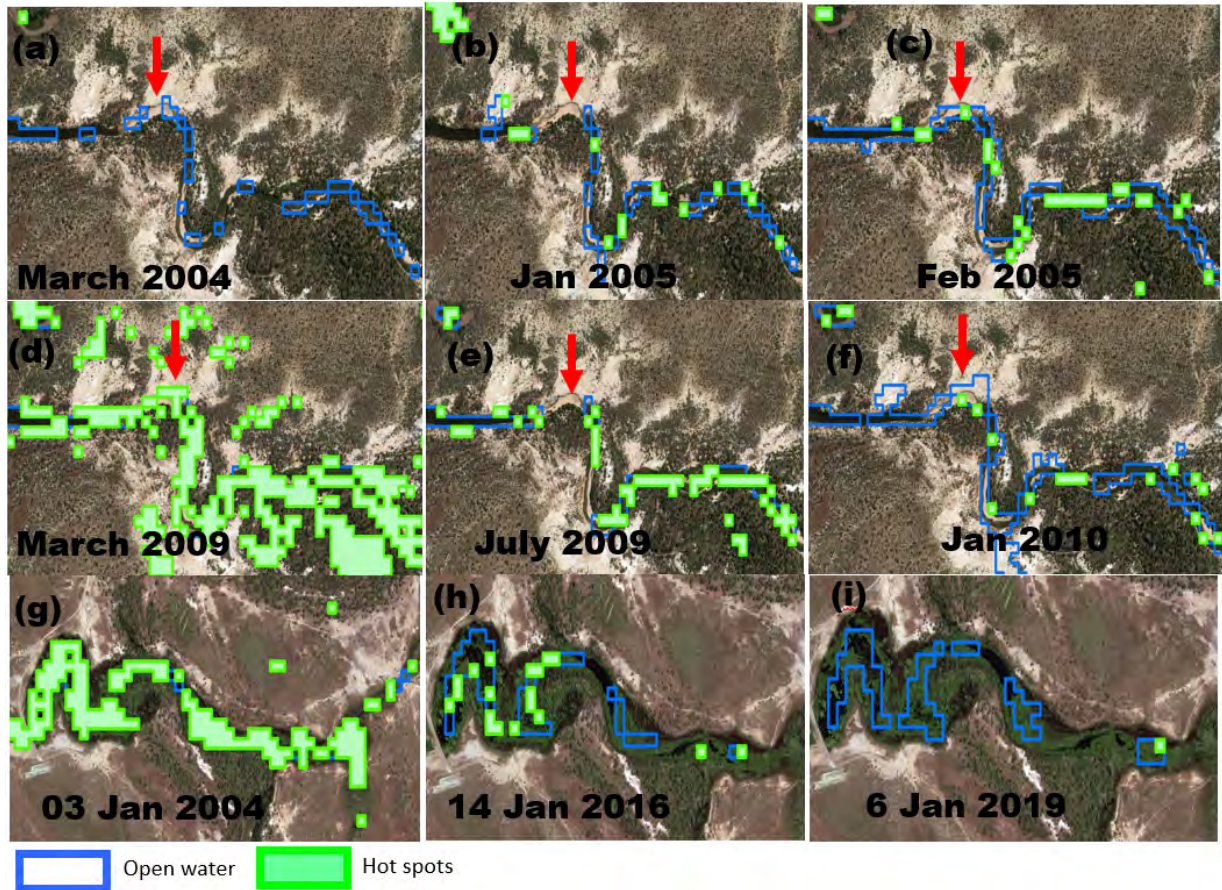
23

Figure 14: The changing characteristics of inundation and impact on the connectivity of freshwater habitats. (a-f) Show the characteristics of inundation in riverine systems and the distribution of hot spots of primary producers while (g-i) are illustrations of the productivity and connectivity of Palustrine systems for January 2004, 2016, and 2019. The background high-resolution satellite imagery is that of Digital Globe captured in May 2015.

waterbodies in wet-dry tropics are characterised by a range of turbidities and land cover states, the abundance of floodplain macrophytes and other forms of epiphytic algae within the vicinity of some of these freshwater habitats in northern Australia have been documented (e.g., Ward et al., 2016). In addition to the apparent presence of algae in larger waterholes in Australian inland floodplains, these waterholes are also highly turbid (e.g., Faggotter et al., 2013; Bunn et al., 2003). The range of turbidities in optically-different freshwater bodies over the Gilbert catchment is evident in their endmember spectra profiles. On the one hand, open water features in locations with aquatic vegetation have different spectral properties and reflectance compared with other open water channels. On the other hand, the spectral characteristics of inland and coastal waters within the same river channel were significantly different. For this reason, there were considerable morphological differences in the riverine systems classified by using these

24

endmember spectra collections in the spectral angle mapper algorithm (Figs. 3g). Compared with this supervised algorithm, the classification tree model gave better results in terms of the extraction of these riverine systems and hot spots of primary production (Figs. 3d and g and 4). Arguably, erosion, pollution, and several other landscape processes could alter the spectral composition of fluxes within these freshwater habitats, and can complicate the spectral separability of these systems. Such complication arises because the unique spectral property of water bodies are compromised by these factors, resulting in different levels of turbidities. This makes most supervised and unsupervised classification algorithms unsuitable for the mapping of aquatic habits and primary production centers (see, Gidley, 2009). Physically-based spectral techniques such as the spectral angle mapper have demonstrated this weakness. Rule-based approaches, as demonstrated in this study, are therefore emerging as reliable alternatives over traditional methods for the assessment of floodplain wetlands and mapping the spatial distribution of aquatic vegetation (e.g., Ward et al., 2014; Zhao et al., 2013; Davranche et al., 2010; Ozesmi and Bauer, 2002).

6.2. Dynamics in tropical floodplains: climate change or human interventions

Changes in tropical floodplains are expected to be driven by inter-annual or seasonal variation in precipitation. These variations in precipitation could sometimes be triggered by multi-scale climate modes and other important processes of inter-annual variability such as the El-Niño Southern Oscillation (see, e.g., Ndehedehe et al., 2019a, 2017; Linage et al., 2013; Phillips et al., 2012). Generally, the above-average precipitation induced by these multi-scale climate oscillations influence local hydrology (e.g., flow dynamics) and result in considerable amplitudes of land water storage in highly productive freshwater ecosystems (e.g., Ndehedehe and Ferreira, 2019). For other tropical systems or wet-dry tropics nonetheless, it may induce high amount of floods on floodplains and freshwater habitats. As highlighted in this study for the period between 1991 and 2019 in the Gilbert catchment, the frequency and intensity of these high-magnitude floods and/or seasonal floodplain inundation could vary within a decade. Strong seasonality in rainfall is a well known climate feature in wet-dry tropical savanna regions. This usually results in short wet seasons that are immediately followed by limited river flows or sometimes none (e.g., Ward et al., 2013). This study confirms that increased variability in annual rainfall of wet-dry tropical areas of Australia will apparently translate into strong dynamics in flow (Fig. 13d). But the influence of rainfall seasonality in the variation of predicted hot spots of primary producers and floodplain inundation in the Gilbert downstream

25

catchment is also noted. However, land use change/land cover change, particularly irrigated agriculture may increase water demand (e.g., Tulbure and Broich, 2019), and other drivers of streamflow characteristics. These drivers, e.g., soil property, topography, and dryness index, which are scale and region dependent (Trancoso et al., 2017) are key factors that could impact on the rainfall-flow interaction in the Gilbert catchment, especially river flow, which may convey nutrients that drive primary production.

The knowledge of climate change as a concept is increasing but it likely impacts, for example, on freshwater ecosystems are still poorly understood. Some pioneering studies (e.g., Mulholland et al., 1997; Bazzaz, 1990) have documented the influence of increasing greenhouse gas concentrations and global warming on the earth's energy budget and natural ecosystems. In the freshwater ecosystems of the south-eastern United States and the Gulf coast of Mexico, for example, climate change has been shown to have ecological consequences, including, rise in the rates of primary production, loss of organisms during strong flushing events in streams and wetlands, amongst several other effects (see, Mulholland et al., 1997). Unfortunately, the impacts of human-induced climate change is expected to exacerbate, resulting in the acceleration of the water cycle and other devastating effects on natural ecosystems, including wetlands, freshwater habitats, and species richness. While repercussions resulting from the alteration of flow regimes on floodplain wetland ecosystems have been detailed (e.g., Bunn and Arthington, 2002), results in this study have shown that rivers, especially in wet-dry tropical savannas with similar topographic layout (Fig. 1a) and rainfall distribution (Fig. 12) could serve as key indicators of floodplain productivity. This argument is further underpinned by the fact that the biota in the wet dry tropics are highly adapted to variable flow conditions (Kingsford et al., 2014).

Indeed, hydro-meteorological fluctuations through changes in climate play critical roles in the observed dynamics of the downstream Gilbert floodplain. The argument for this is two fold. First, the stream water levels (maximum and monthly show correlations of 0.87 and 0.83, respectively with rainfall) of the downstream catchment and their cumulative departures ($r = 0.96$) show considerable agreement with averaged rainfall over the entire Gilbert catchment. This also implies that changes in rainfall (i.e., decline or increase) over Gilbert will impact stream water levels and floodplain inundation in general. This applies to river flow and has been demonstrated for 2009 (Supporting information, S1), the wettest period on record in over two decades. Second, the leading rainfall mode localised over the downstream catchment (PC-1, Fig. 12) was associated with observed river discharge ($r = 0.83$ or $R^2 = 68\%$) and

26

stream water levels ($r = 0.68$ or $R^2 = 47\%$) at Gilbert downstream. Moreover, the gauge rainfall records of downstream Gilbert indicate that variations in floodplain inundation are also induced by the local rainfall amounts of previous months. We found this phenomenon to be true also for wet season discharge, for example in March 2005, 2009, and 2010. While taking note of probable uncertainties in the estimated extents of hot spots due to impact of cloud, the flow-hot spot relationship ($r = 0.68$ at one month lag) of the Gilbert catchment, is obviously moderately higher than the local rainfall-hot spot association ($r = 0.57$ at three months lag). This result is consistent with earlier reports on the perceived influence of flow on aquatic biodiversity (e.g., Bunn et al., 2006) and is also crucial for further discussions on the impacts of flow alterations on the productivity of floodplain rivers. Generally, the evidence of this composite influence of downstream rainfall and flow on the dynamics of floodplain productivity in downstream Gilbert underscores the role of upstream catchment in driving the downstream floodplain inundation and primary production. In the event of major water resources development along the upstream floodplains or change in government water-related policies, we argue that such developments could amplify flow variability, resulting in significant impacts on freshwater habits and hot spots of primary producers.

6.3. Freshwater needs for the sustainability of floodplain productivity and aquatic biodiversity

A global scale simulation of the impacts of climate change on freshwater ecosystems highlights the important roles of climate and water infrastructures on ecologically relevant river flow characteristics, arguing that by 2050 climate change will have more impact on river flow alteration compared with dam construction (Döll and Zhang, 2010). Emerging economies who depend on hydro-power suffer shortages or lack of electricity during extreme drought periods, which impacts on flow dynamics and in turn limits/reduce reservoir storage (e.g., Ndehedehe, 2019). This is obviously a negative impact of climate change and/or variability on surface hydrology these economies have to cope with during such times. Changes in precipitation patterns caused by rising temperatures and changes in atmospheric circulation patterns result in considerable influence on hydrology at different spatial and temporal scales. These important climate components and its dynamics do not only impact on ecosystems (Woodward et al., 2010), but could also interact with other anthropogenic or human stressors that make freshwater habitats even more vulnerable to climate change. This was the case in Lake Chad where intensive water extraction from the Lake for irrigation purposes compounded the effects of prolonged extreme droughts, culminating in considerable contraction of the Lake Chad's

27

surface area (e.g., Ndehedehe, 2019).

In the Australian wet-dry tropics, the importance of flow regimes in ecological processes such as fish migration patterns, habitat availability, in-channel interactions with other systems has been highlighted (e.g., Kingsford et al., 2014; Bunn and Arthington, 2002). The influence of flow variability on aquatic production and food availability for fish and other consumers was identified in the Australian dryland rivers (e.g., Bunn et al., 2006). Even water holes around the vicinity of such rivers, which were found to be characterised by extreme flow variability supported a plethora of fish fauna after high summer flows while fewer species and lower numbers of fish catch were recorded during periods of low flow (Balcombe and Arthington, 2009). Arguably, a high level of connectivity between these rivers and intermittent water holes as is usually the case in extreme wet summers is required to sustain aquatic biodiversity, fish populations and other higher level consumers. However, it has been argued that water resource development in dryland rivers could impact on sources of production due to increase in the frequency and duration of in-channel flows despite its role in the physical persistence and connectivity of these waterholes (see, Bunn et al., 2006). In addition to the increasing pressure from water resource development in the floodplain wetlands of Australian wet–dry tropics (e.g., Ward et al., 2013), the hydrological regimes of river–floodplain systems in are usually modified by human societies because of the need to provide important ecological services, which include recreation, water supply, production of hydropower, flood control, among others (e.g., Kennard et al., 2010). In Australia, these services and other multiple streams of anthropogenic influence, including the degradation of riparian areas were identified as significant threats to freshwater ecosystems, necessitating conservation protection through a proposed establishment of a system of freshwater reserve (e.g., Fitzsimons and Robertson, 2005). This human footprint and the impacts of rainfall seasonality and key hydrological metrics (e.g., extent, timing, duration, and amplitude), which regulates the exchange of water fluxes within freshwater habits and the growth of aquatic plants highlight the need for sustainability of water resources in the region. With about 93% of the total annual rainfall occurring during the wet season and 84% of rainfall being lost to evaporation in the Gilbert catchment (CSIRO, 2013), sustainability of freshwater ecosystems in this region will be underpinned by frequent monitoring of large-scale freshwater habitats. The large-scale assessment of these remote floodplains using improved optical remote sensing methods is therefore a primary initiative that can be taken as a first step to support management and water resources planning.

28

7. Conclusions

In the assessment of floodplain productivity and freshwater habitats in a large floodplain river in northern Australia, results in this study reveal that:

(i) In terms of floodplain inundation and the spatial distribution of hot spots, the most productive period in the catchment since 1991 to date (from available landsat data) was the period between 1998 and 2010. The dearth of aquatic primary production (hot spots) in relatively dry years or during dry spells (periods during $1993 - 1997$ and $2014 - 2019$, excluding 2018 and other years affected by clouds) is in sharp contrast to the abundant distribution of hot spots during productive years in the catchment. The connectivity of slightly isolated water holes and other intermittent water bodies to adjacent rivers during such productive and extreme wet periods (e.g, 2009) could last up to 4 months and more.

(ii) Rainfall seasonality is a critical indicator of the spatial distribution of floodplain inundation in the Gilbert catchment of northern Australia. However, peak correlation of downstream discharge with estimated hot spots of primary production (phase lag < one month) is relatively higher than the observed maximum association of rainfall with hot spots at three months phase lags. The considerable agreement ($r = 0.83$) between the dominant pattern of rainfall (inter-annual fluctuations) over the entire Gilbert catchment and downstream discharge provides further clue to the importance of rivers in the evolution of hot spots of primary producers. The interactions of anthropogenic stressors (e.g., water resources development along floodplains) with key climate components (e.g., precipitation and discharge) can amplify this relationship to the detriment of the ecological services provided by these rivers. Local rainfall however, appears to be a better predictor of downstream inundation ($r = 0.71$ @ lag=0) as opposed to discharge ($r = 0.65$ @ lag=1).

(iii) The association of wet season rainfall anomalies over the Gilbert catchment with water level anomalies in the river ($r = 0.83$) (or maximum monthly water level anomalies-$r = 0.87$) and discharge at the downstream catchment is high and significant. The monthly cumulative departures of averaged wet season Gilbert rainfall is also strongly associated with downstream wet season stream water levels ($r = 0.96$). Put together, this confirms on the one hand, the explicit contributions of upstream catchment to

29

downstream floodplain productivity. On the other hand, it also implies that hydro-meteorological fluctuations through changes in climate play critical roles in the characteristics of downstream Gilbert floodplain inundation, which in turn impacts the connectivity of freshwater habitats and distribution of aquatic vegetation.

(iv) Finally, in the delineation of inundation patterns and identification of hot spots of primary producers (inundated areas covered with different aquatic species such as macrophytes) over large tropical floodplains, where waterbodies have a range of turbidities, rule-based approaches are more reliable as opposed to traditional and pixel-based methods. By combining vegetation and inundation metrics in a classification tree model, this was demonstrated for the Gilbert catchment in northern Australia where the spectral composition of fluxes complicated the spectral separability of freshwater systems using pixel-based methods such as the spectral angle mapper.

Overall, the scope of this study was limited by data gaps (non-availability of wet season images for some months) and the impacts of cloud, which affected some wet season landsat imageries of the Gilbert catchment. This could impact on the interpretation of results (e.g., estimated inundation extent will be lower because of images flagged for clouds) for some years (e.g., January 2009) with major flood events. Despite this constraint, statistical relationships developed between hydrological and extents of hot spots of aquatic primary producers are adequate to guide water-related policy and the development of climate change mitigation and resource management strategies.

8. Supporting Information: Characteristics of the 2009 daily river discharge and stream water level observations
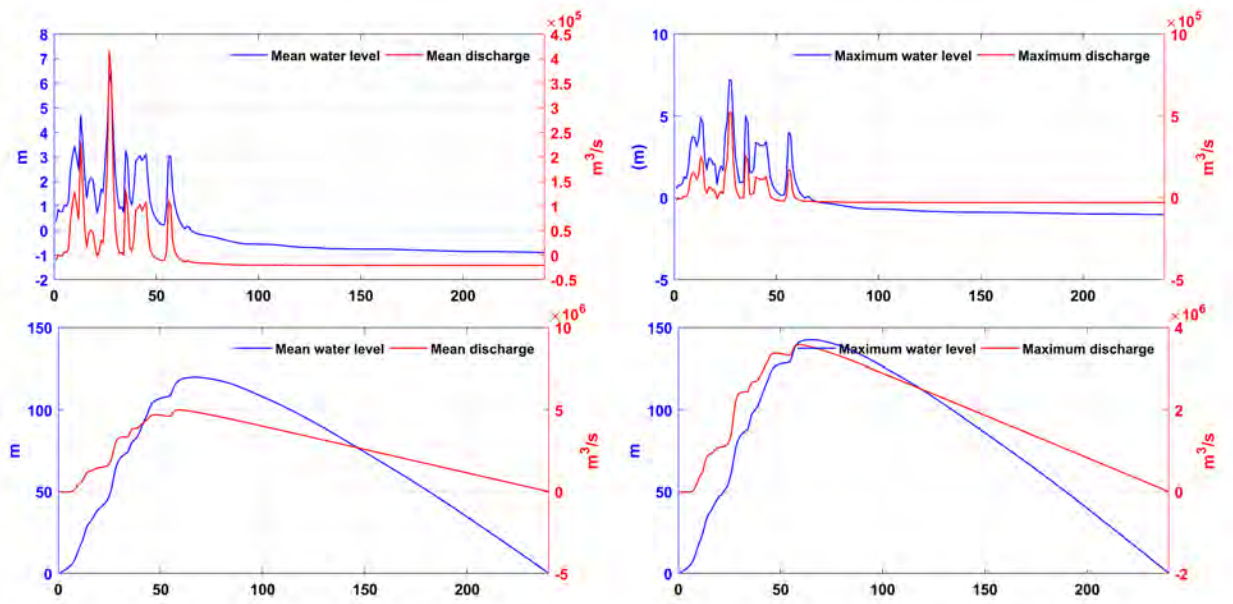
Figure 15: Daily river discharge and stream water levels of 2009 (January-August), the year with high density, mega flood in much of the wet-dry tropics of northern Australia. The top panels show anomalies in mean and maximum river discharge and stream water levels while the bottom panel indicates cumulative departures of the same quantities. The gauge records are taken from Rockfield station downstream Gilbert catchment.

References

Agutu, N., Awange, J., Zerihun, A., Ndehedehe, C., Kuhn, M., and Fukuda, Y. (2017). Assessing multi-satellite remote sensing, reanalysis, and land surface models' products in characterizing agricultural drought in East Africa. *Remote Sensing of Environment*, 194(0):287–302. doi:10.1016/j.rse.2017.03.041.

Balcombe, S. R. and Arthington, A. H. (2009). Temporal changes in fish abundance in response to hydrological variability in a dryland floodplain river. *Marine and Freshwater Research*, 60:146–159. doi:10.1071/MF08118.

Barberm, M., Waltham, N., Burrows, D., Brennan, M. L., Crossman, N., Petheram, C., Higgins, A., Marston, F., Buettikofer, H., Reedman, L., Banerjee, O., and Wallbrink, A. (2013). Chapter 4: Living and built environment of the gilbert catchment. in: Petheram c, watson i and stone p (eds) agricultural resource assessment for the gilbert catchment. *A report to the Australian Government from the CSIRO Flinders and Gilbert Agricultural Resource Assessment, part of the North Queensland Irrigated Agriculture Strategy.* CSIRO Water for a Healthy Country and Sustainable Agriculture flagships, Australia. Accessed online on 14th August, 2019.

Bazzaz, F. A. (1990). The response of natural ecosystems to the rising global CO2 levels. *Annual Review of Ecology and Systematics*, 21(1):167–196. doi:10.1146/annurev.es.21.110190.001123.

Bernstein, L. S., Adler-Golden, S. M., Jin, X., Gregor, B., and Sundberg, R. L. (2012). Quick atmospheric correction (quac) code for vnir-swir spectral imagery: Algorithm details. In *2012 4th Workshop on Hyperspectral Image and Signal Processing: Evolution in Remote Sensing (WHISPERS)*, pages 1–4. doi:10.1109/WHISPERS.2012.6874311.

Bernstein, L. S., Adler-Golden, S. M., Sundberg, R. L., Levine, R. Y., Perkins, T. C., Berk, A., Ratkowski, A. J., Felde, G., and Hoke, M. L. (2005). A new method for atmospheric correction and aerosol optical property retrieval for VIS-SWIR multi- and hyperspectral imaging sensors: QUAC (QUick atmospheric correction). In *Proceedings. 2005 IEEE International Geoscience and Remote Sensing Symposium, 2005. IGARSS '05.*, volume 5, pages 3549–3552.

Brillinger, D. R. (2004). Some data analyses using mutual information. *Brazilian Journal of Probability and Statistics*, 18(2):163–182.

Bunn, S., Ward, D., Crook, D., Jardine, T., Pettit, N., Douglas, M., and Kyne, P. (2015). Tropical floodplain food webs - connectivity and hotspots. *Darwin: Charles Darwin University.*

Bunn, S. E. and Arthington, A. H. (2002). Basic principles and ecological consequences of altered flow regimes for aquatic biodiversity. *Environmental Management*, 30(4):492–507. doi:10.1007/s00267-002-2737-0.

Bunn, S. E., Davies, P. M., and Winning, M. (2003). Sources of organic carbon supporting the food web of an arid zone floodplain river. *Freshwater Biology*, 48(4):619–635. doi:10.1046/j.1365-2427.2003.01031.x.

Bunn, S. E., Thoms, M. C., Hamilton, S. K., and Capon, S. J. (2006). Flow variability in dryland rivers: boom, bust and the bits in between. *River Research and Applications*, 22(2):179–186. doi:10.1002/rra.904.

Chander, G., Markham, B. L., and Helder, D. L. (2009). Summary of current radiometric calibration coefficients for Landsat MSS, TM, ETM+, and EO-1 ALI sensors. *Remote Sensing of Environment*, 113(5):893 – 903.

Chen, Q., Yu, R., Hao, Y., Wu, L., Zhang, W., Zhang, Q., and Bu, X. (2018). A new method for mapping aquatic vegetation especially underwater vegetation in Lake Ulansuhai Using GF-1 satellite data. *Remote Sensing*, 10(8). doi:10.3390/rs10081279.

Chen, T., de Jeu, R., Liu, Y., van der Werf, G., and Dolman, A. (2014a). Using satellite based soil moisture to quantify the water driven variability in NDVI: A case study over mainland Australia. *Remote Sensing of Environment*, 140:330 – 338. doi:10.1016/j.rse.2013.08.022.

Chen, Y., Wang, B., Pollino, C. A., Cuddy, S. M., Merrin, L. E., and Huang, C. (2014b). Estimate of flood inundation and retention on wetlands using remote sensing and GIS. *Ecohydrology*, 7(5):1412–1420. doi:10.1002/eco.1467.

Cho, H. J., Kirui, P., and Natarajan, H. (2008). Test of multi-spectral vegetation index for floating and canopy-forming submerged vegetation. *International journal of environmental research and public health*, 5(5):477–483.

Congalton, R. and Green, K. (2009). *Assessing the Accuracy of Remotely Sensed Data: Principles and Practices*. Taylor & Francis, 2nd edition.

CSIRO (2013). Agricultural resource assessment for the gilbert catchment. an overview report to the australian government from the CSIRO Flinders and Gilbertagricultural resource assessment, part of the north queensland irrigated agriculture strategy. *CSIRO*. CSIRO Water for a Healthy Country and Sustainable Agriculture flagships, Australia. Accessed online on 14th August, 2019.

Davranche, A., Lefebvre, G., and Poulin, B. (2010). Wetland monitoring using classification trees and SPOT-5seasonal time series. *Remote Sensing of Environment*, 114(3):552 – 562. doi:10.1016/j.rse.2009.10.009.

Döll, P. and Zhang, J. (2010). Impact of climate change on freshwater ecosystems: a global-scale analysis of ecologically relevant river flow alterations. *Hydrology and Earth System Sciences*, 14(5):783–799.

Faggotter, S. J., Webster, I. T., and Burford, M. A. (2013). Factors controlling primary productivity in a wet–dry tropical river. *Marine and Freshwater Research*, 64:585–598. doi:10.1071/MF12299.

Ferreira, V., Montecino, H., Ndehedehe, C., Heck, B., Gong, Z., Westerhaus, M., and de Freitas, S. (2018). Space-based observations of crustal deflections for drought characterization in brazil. *Science of The Total Environment*, 644:256–273. doi:10.1016/j.scitotenv.2018.06.277.

Feyisa, G. L., Meilby, H., Fensholt, R., and Proud, S. R. (2014). Automated water extraction index: A new technique for surface water mapping using landsat imagery. *Remote Sensing of Environment*, 140:23 – 35. doi:10.1016/j.rse.2013.08.029.

Fisher, A., Flood, N., and Danaher, T. (2016). Comparing landsat water index methods for automated water classification in eastern Australia. *Remote Sensing of Environment*, 175:167 – 182. doi:10.1016/j.rse.2015.12.055.

Fitzsimons, J. A. and Robertson, H. A. (2005). Freshwater reserves in Australia: Directions and challenges for the development of a comprehensive, adequate and representative system of protected areas. *Hydrobiologia*, 552(1):87–97. doi:10.1007/s10750-005-1507-4.

Frappart, F., Papa, F., da Silva, J. S., Ramillien, G., Prigent, C., Seyler, F., and Calmant, S. (2012). Surface freshwater storage and dynamics in the Amazon basin during the 2005 exceptional drought. *Environmental Research Letters*, 7(4):044010.

Gidley, S. L. (2009). Using high resolution satellite imagery to map aquatic macrophytes on multiple lakes in northern indiana. *Unpublished Msc thesis, Indiana University*. Retrieved from https://core.ac.uk/download/pdf/46956355.pdf on 15th April, 2019.

Karim, F., Kinsey-Henderson, A., Wallace, J., Arthington, A. H., and Pearson, R. G. (2012). Modelling wetland connectivity during overbank flooding in a tropical floodplain in north Queensland, Australia. *Hydrological Processes*, 26(18):2710–2723. doi:10.1002/hyp.8364.

Karim, F., Peña-Arancibia, J., Ticehurst, C., Marvanek, S., Gallant, J., Hughes, J., Dutta, D., Vaze, J., C, P., Seo, L., and Kitson, S. (2018). Floodplain inundation mapping and modelling for the fitzroy, darwin and mitchell catchments. a technical report to the australian government from the csiro northern australia water resource assessment, part of the national water infrastructure development fund: Water resource assessments. *CSIRO, Australia.*

Keddy, P. A., Fraser, L. H., Solomeshch, A. I., Junk, W. J., Campbell, D. R., Arroyo, M. T. K., and Alho, C. J. R. (2009). Wet and Wonderful: The World's Largest Wetlands Are Conservation Priorities. *BioScience*, 59(1):39–51. doi:10.1525/bio.2009.59.1.8.

Kennard, M. J., Pusey, Bradley J.and Olden, J. D., Mackay, S. J., Stein, J. L., and Marsh, N. (2010). Classification of natural flow regimes in Australia to support environmental flow management. *Freshwater Biology*, 55(1):171–193. doi:10.1111/j.1365-2427.2009.02307.x.

Khandelwal, A., Karpatne, A., Marlier, M. E., Kim, J., Lettenmaier, D. P., and Kumar, V. (2017). An approach for global monitoring of surface water extent variations in reservoirs using modis data. *Remote Sensing of Environment*, 202:113 – 128. doi:10.1016/j.rse.2017.05.039.

Kim, D., Lee, H., Laraque, A., Tshimanga, R. M., Yuan, T., Jung, H. C., Beighley, E., and Chang, C.-H. (2017). Mapping spatio-temporal water level variations over the central congo river using palsar scansar and envisat altimetry data. *International Journal of Remote Sensing*, 38(23):7021–7040. doi:10.1080/01431161.2017.1371867.

Kingsford, R., Watts, R., Keohn, J., Thompson, R., and Sims, N. (2014). Flow dependent ecological responses. a technical report from the ecological responses to altered flow regimes

flagship research cluster (subproject 3). *CSIRO Water for a Healthy Country Flagship, Australia.*

Kruse, F., Lefkoff, A., Boardman, J., Heidebrecht, K., Shapiro, A., Barloon, P., and Goetz, A. (1993). The spectral image processing system (SIPS)—interactive visualization and analysis of imaging spectrometer data. *Remote Sensing of Environment*, 44(2):145 – 163. doi:10.1016/0034-4257(93)90013-N.

Lee, H., Jung, H. C., Yuan, T., Beighley, R. E., and Duan, J. (2014). Controls of terrestrial water storage changes over the Central Congo Basin determined by integrating Palsar ScanSar, Envisat Altimetry, and Grace data. *Remote Sensing of the Terrestrial Water Cycle, Geophysical Monograph*, 206:117–129. doi:10.1002/9781118872086.ch7/pdf.

Linage, C., Kim, H., Famiglietti, J. S., and Yu, J.-Y. (2013). Impact of pacific and atlantic sea surface temperatures on interannual and decadal variations of GRACE land water storage in tropical South America. *Journal of Geophysical Research: Atmospheres*, 118(19):10,811–10,829. doi:10.1002/jgrd.50820.

Midwood, J. D. and Chow-Fraser, P. (2010). Mapping floating and emergent aquatic vegetation in coastal wetlands of eastern georgian bay, lake huron, canada. *Wetlands*, 30(6):1141–1152. doi:10.1007/s13157-010-0105-z.

Moon, Y.-I., Rajagopalan, B., and Lall, U. (1995). Estimation of mutual information using kernel density estimators. *Phys. Rev. E*, 52:2318–2321. doi:10.1103/PhysRevE.52.2318.

Mulholland, P. J., Best, G. R., Coutant, C. C., Hornberger, G. M., Meyer, J. L., Robinson, P. J., Stenberg, J. R., Turner, R. E., Vera-Herrera, F., and Wetzel, R. G. (1997). Effects of climate change on freshwater ecosystems of the south-eastern United States and the gulf coast of Mexico. *Hydrological Processes*, 11(8):949–970. doi:10.1002/(SICI)1099-1085(19970630)11:8<949::AID-HYP513>3.0.CO;2-G.

Ndehedehe, C. E. (2019). The water resources of tropical West Africa: propblems, progress and prospect. *Acta Geophysica*, 67(2):621–649. https://doi.org/10.1007/s11600-019-00260-y.

Ndehedehe, C. E., Anyah, R. O., Alsdorf, D., Agutu, N. O., and Ferreira, V. G. (2019a). Modelling the impacts of global multi-scale climatic drivers on hydro-climatic extremes (1901–2014) over the Congo basin. *Science of The Total Environment*, 651:1569 – 1587. doi:10.1016/j.scitotenv.2018.09.203.

Ndehedehe, C. E., Awange, J., Kuhn, M., Agutu, N., and Fukuda, Y. (2017). Climate tele-connections influence on West Africa's terrestrial water storage. *Hydrological Processes*, 31(18):3206–3224. doi: 10.1002/hyp.11237.

Ndehedehe, C. E. and Ferreira, V. G. (2019). Identifying the footprints of global climate modes in time-variable gravity hydrological signals. *Climatic Change*.

Ndehedehe, C. E., Ferreira, V. G., and Agutu, N. O. (2019b). Hydrological controls on surface vegetation dynamics over West and Central Africa. *Ecological Indicators*, 103:494 – 508. doi:10.1016/j.ecolind.2019.04.032.

Normandin, C., Frappart, F., Lubac, B., Bélanger, S., Marieu, V., Blarel, F., Robinet, A., and Guiastrennec-Faugas, L. (2018). Quantification of surface water volume changes in the Mackenzie Delta using satellite multi-mission data. *Hydrology and Earth System Sciences*, 22(2):1543–1561.

Ozesmi, S. L. and Bauer, M. E. (2002). Satellite remote sensing of wetlands. *Wetlands Ecology and Management*, 10(5):381–402. doi:10.1023/A:1020908432489.

Phillips, T., Nerem, R. S., Fox-Kemper, B., Famiglietti, J. S., and Rajagopalan, B. (2012). The influence of ENSO on global terrestrial water storage using GRACE. *Geophysical Research Letters*, 39:L16705. doi:10.1029/2012GL052495, 2012.

Preisendorfer, R. (1988). Principal component analysis in meteorology and oceanography. *Developments in Atmospheric Science 17*. Elsevier, Amsterdam.

Sakamoto, T., Nguyen, N. V., Kotera, A., Ohno, H., Ishitsuka, N., and Yokozawa, M. (2007). Detecting temporal changes in the extent of annual flooding within the Cambodia and the Vietnamese Mekong Delta from MODIS time-series imagery. *Remote Sensing of Environment*, 109(3):295 – 313.

Sharma, A. (2000). Seasonal to interannual rainfall probabilistic forecasts for improved water supply management: Part 1 — a strategy for system predictor identification. *Journal of Hydrology*, 239(1):232 – 239. doi:10.1016/S0022-1694(00)00346-2.

Snedecor, G. W. and Cochran, W. G. (1989). Statistical methods. *Iowa State University Press*, 8th Edition.

Song, C., Woodcock, C. E., Seto, K. C., Lenney, M. P., and Macomber, S. A. (2001). Classification and change detection using landsat TM data: When and how to correct atmospheric effects? *Remote Sensing of Environment*, 75(2):230 – 244. doi:doi:10.1016/S0034-4257(00)00169-3.

Syvitski, J. P., Overeem, I., Brakenridge, G. R., and Hannon, M. (2012). Floods, floodplains, delta plains — a satellite imaging approach. *Sedimentary Geology*, 267-268:1 – 14. doi:10.1016/j.sedgeo.2012.05.014.

Tapley, B., Bettadpur, S., Watkins, M., and Reigber, C. (2004). The Gravity Recovery and Climate Experiment: Mission overview and early results. *Geophysical Research Letters*, 31:1–4. doi:10.1029/ 2004GL019920.

Tockner, K., Lorang, M. S., and Stanford, J. A. (2010). River flood plains are model ecosystems to test general hydrogeomorphic and ecological concepts. *River Research and Applications*, 26(1):76–86. doi:10.1002/rra.1328.

Trancoso, R., Phinn, S., McVicar, T. R., Larsen, J. R., and McAlpine, C. A. (2017). Regional variation in streamflow drivers across a continental climatic gradient. *Ecohydrology*.

Tulbure, M. G. and Broich, M. (2019). Spatiotemporal patterns and effects of climate and land use on surface water extent dynamics in a dryland region with three decades of Landsat satellite data. *Science of The Total Environment*, 658:1574 – 1585. doi:10.1016/j.scitotenv.2018.11.390.

Tulbure, M. G., Broich, M., Stehman, S. V., and Kommareddy, A. (2016). Surface water extent dynamics from three decades of seasonally continuous landsat time series at subcontinental scale in a semi-arid region. *Remote Sensing of Environment*, 178:142 – 157. doi:10.1016/j.rse.2016.02.034.

Waltham, N., Burrows, D., Butler, B., Wallace, J., Thomas, C., James, C., and Brodie, J. (2013). Waterhole ecology in the Flinders and Gilbert catchments. A technical report to the Australian Government from the CSIRO Flinders and Gilbert Agricultural Resource Assessment, part of the North Queensland Irrigated Agriculture Strategy. CSIRO Water for a Healthy Country and Sustainable Agriculture flagships, Australia.

Ward, D., Petty, A., Setterfield, S., Douglas, M., Ferdinands, K., Hamilton, S., and Phinn, S. (2014). Floodplain inundation and vegetation dynamics in the alligator rivers region

(kakadu) of northern australia assessed using optical and radar remote sensing. *Remote Sensing of Environment*, 147:43 – 55. doi:10.1016/j.rse.2014.02.009.

Ward, D. P., Hamilton, S. K., Jardine, T. D., Pettit, N. E., Tews, E. K., Olley, J. M., and Bunn, S. E. (2013). Assessing the seasonal dynamics of inundation, turbidity, and aquatic vegetation in the australian wet–dry tropics using optical remote sensing. *Ecohydrology*, 6(2):312–323. doi:10.1002/eco.1270.

Ward, D. P., Pettit, N. E., Adame, M., Douglas, M. M., Setterfield, S. A., and Bunn, S. E. (2016). Seasonal spatial dynamics of floodplain macrophyte and periphyton abundance in the Alligator Rivers region (Kakadu) of northern Australia. *Ecohydrology*, 9(8):1675–1686. doi:10.1002/eco.1757.

Woodward, G., Perkins, D. M., and Brown, L. E. (2010). Climate change and freshwater ecosystems: impacts across multiple levels of organization. *Philosophical Transactions of the Royal Society B: Biological Sciences*, 365(1549):2093–2106. doi:10.1098/rstb.2010.0055.

Xu, H. (2006). Modification of normalised difference water index (NDWI) to enhance open water features in remotely sensed imagery. *International Journal of Remote Sensing*, 27(14):3025–3033. doi:10.1080/01431160600589179.

Zhao, D., Jiang, H., Yang, T., Cai, Y., Xu, D., and An, S. (2012). Remote sensing of aquatic vegetation distribution in Taihu Lake using an improved classification tree with modified thresholds. *Journal of Environmental Management*, 95(1):98 – 107. doi:10.1016/j.jenvman.2011.10.007.

Zhao, D., Lv, M., Jiang, H., Cai, Y., Xu, D., and An, S. (2013). Spatio-temporal variability of aquatic vegetation in Taihu Lake over the past 30 years. *PLOS ONE*, 8(6):1–7. doi:10.1371/journal.pone.0066365.

Zhu, Z., Wang, S., and Woodcock, C. E. (2015). Improvement and expansion of the fmask algorithm: cloud, cloud shadow, and snow detection for landsats 4–7, 8, and sentinel 2 images. *Remote Sensing of Environment*, 159:269 – 277. doi:10.1016/j.rse.2014.12.014.